Tectonics

RESEARCH ARTICLE
10.1029/2017TC004946

The Crustal Domains of the Alboran Basin (Western Mediterranean)

Laura Gómez de la Peña[1,2], César R. Ranero[1,3], and Eulàlia Gràcia[1]

[1]Barcelona Center for Subsurface Imaging, Institut de Ciències del Mar, CSIC, Barcelona, Spain, [2]Now at GEOMAR Helmholtz Centre of Ocean Research, Kiel, Germany, [3]ICREA, Barcelona, Spain

Key Points:
- Four crustal domains are recognized with deep seismic profiles, with basement ground-truth and available drill and dredge samples
- Distribution of domains is consistent with formation of a subduction system that includes a fore-arc, a magmatic arc, and a back-arc basin
- Present-day large active tectonic structures are nucleated at the boundaries between different crustal domains

Supporting Information:
- Supporting Information S1

Correspondence to:
L. Gómez de la Peña,
lgomez@geomar.de

Citation:
Gómez de la Peña, L., Ranero, C. R., & Gràcia, E. (2018). The crustal domains of the Alboran Basin (western Mediterranean). *Tectonics*, *37*, 3352–3377. https://doi.org/10.1029/2017TC004946

Received 5 JAN 2018
Accepted 18 AUG 2018
Accepted article online 28 AUG 2018
Published online 2 OCT 2018

Abstract The Alboran Basin in the westernmost Mediterranean hosts the orogenic boundary between the Iberian and African plates. Although numerous geophysical studies of crustal structure onshore Iberia have been carried out during the last decade, the crustal structure of the Alboran Basin has comparatively been poorly studied. We analyze crustal-scale images of a grid of new and reprocessed multichannel seismic profiles showing the tectonic structure and variations in the reflective character of the crust of the basin. The nature of the distinct domains has been ground-truthed using available basement samples from drilling and dredging. Our results reveal four different crustal types—domains—of the Alboran Basin: (a) a thin continental crust underneath the West Alboran and Malaga basins, which transitions to (b) a magmatic arc crust in the central part of the Alboran Sea and the East Alboran Basin; (c) the North African continental crust containing the Pytheas and Habibas subbasins; and (d) the oceanic crust in the transition toward the Algero-Balearic Basin. The Alboran Basin crust is configured in a fore-arc basin (West Alboran and Malaga basins), a magmatic arc (central and East Alboran), and a back-arc system in the easternmost part of the East Alboran Basin and mainly Algero-Balearic Basin. The North African continental crust is influenced by arc-related magmatism along its edge and was probably affected by strike-slip tectonics during westward migration of the Miocene subduction system. The distribution of active tectonic structures in the current compressional setting generally corresponds to boundaries between domains, possibly representing inherited lithospheric-scale weak structures.

1. Introduction

The Alboran Basin is located at the westernmost Mediterranean, at the inner part of the Gibraltar Arc system, formed by the Betics and Rif orogenic belts on-land, and the Gulf of Cadiz imbricated wedge toward the west (Gràcia, Dañobeitia, Vergés, Bartolome, 2003; Iribarren et al., 2007; Figure 1). Seismic tomography detected a slab in the upper mantle, which supports that its origin is related to a subduction system (Wortel & Spakman, 2000).

Although the crustal thickness and upper mantle structure under the emerged region around the Alboran Basin has been extensively studied recently using passive seismology methods including travel-time earthquake tomography (e.g., Bezada et al., 2013), surface-wave tomography (e.g., Palomeras et al., 2014), and receiver functions (e.g., Mancilla et al., 2015), the crustal and upper mantle structure under the Alboran Basin still remains inadequately constrained. Results from global travel-time tomography yield mantle structure only where very good ray coverage controls hundreds of kilometers of wavelength features, due to a limited resolution of the method (Chertova et al., 2014; Spakman & Wortel, 2004; Wortel & Spakman, 2000). More recent velocity models obtained with waveform inversion from regional earthquakes (Fichtner & Villaseñor, 2015) show long-wavelength crustal thickness and upper mantle structure. There are few previous deep-penetration multichannel seismic reflection (MCS) studies of the structure of the basin (Booth-Rea et al., 2007; Watts et al., 1993). These data were collected before multibeam bathymetric mapping of the entire basin was available (Ballesteros et al., 2008; d'Acremont et al., 2014; Gràcia, Dañobeitia, Vergés, & Parsifal Team, 2003; Gràcia et al., 2006, 2012; Martinez-Loriente et al., 2016), so that location of seismic profiles is often not optimal. Available basement dredges and scientific and commercial well data samples of basement are scarce but provide key ground-truth information for the domains.

Here we present the first comprehensive study of the Alboran Basin crust characterization derived from MCS images, originally designed and acquired with the objective of imaging the full crustal structure, and

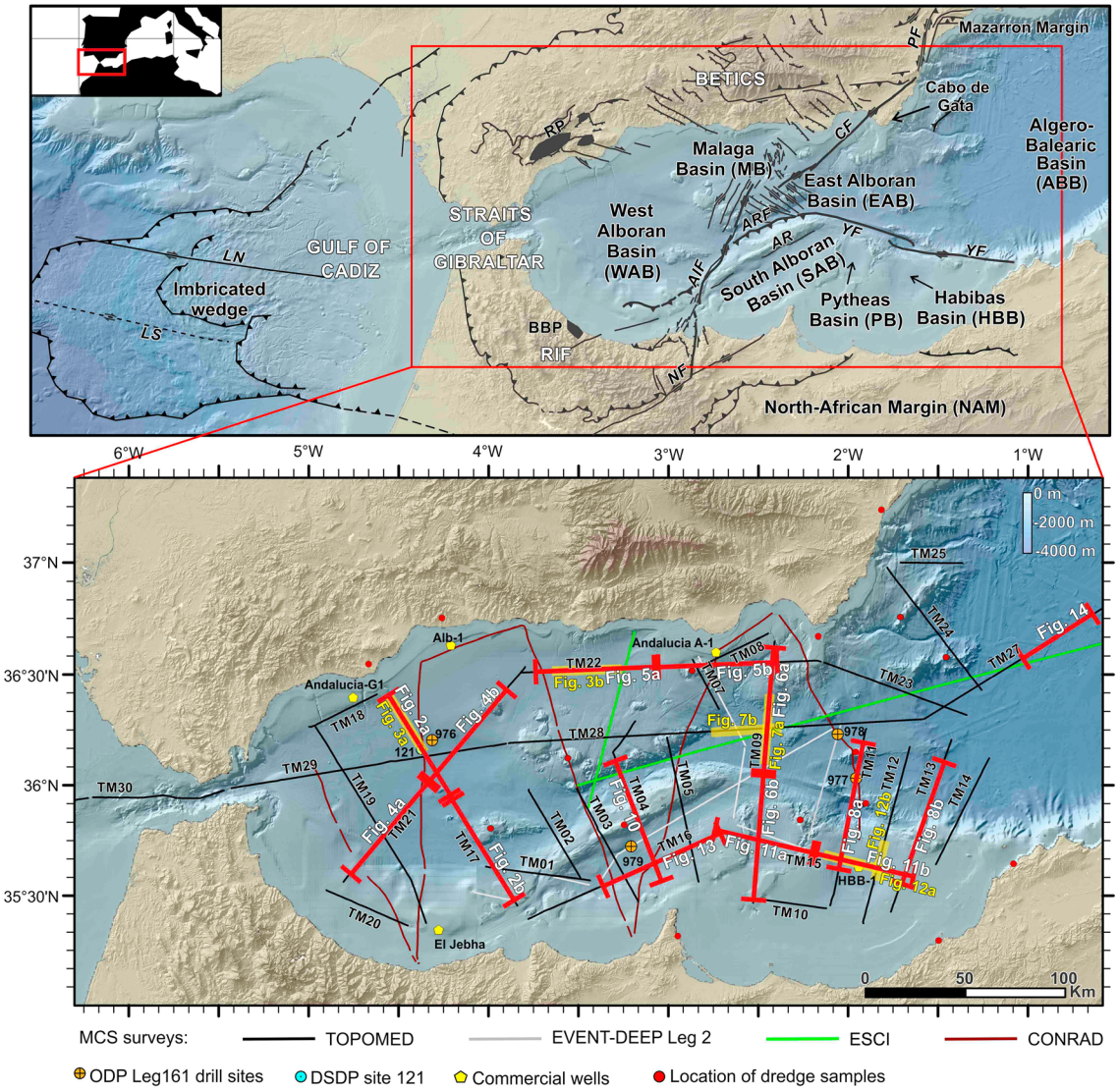

Figure 1. Regional bathymetric map of the Alboran Sea and of the Gulf of Cadiz (d'Acremont et al., 2014; Gràcia, Dañobeitia, Vergés, & Parsifal Team, 2003; Gràcia et al., 2006, 2012; Martínez-Loriente et al., 2013, 2016) completed with IEO bathymetry (Ballesteros et al., 2008; Gómez de la Peña et al., 2016) and released SRTM-3 and GEBCO digital data. Main depocenters and tectonic structures are displayed (Gràcia et al., 2006, 2012). Location of TOPOMED-GASSIS (black lines), EVENT-DEEP Leg 2 (gray lines), ESCI Alboran (green lines), and CONRAD (brown lines) are depicted. Red and yellow lines display the seismic profiles presented in this study. Inset: location of the shown area (red rectangle). AIF = Al-Idrissi Fault; AR = Alboran Ridge; ARF = Alboran Ridge Front Fault; BBP = Beni Bousera Peridotite; CF = Carboneras Fault; LN = Lineation North; LS = Lineation South; NF = Nekor Fault; PF = Palomares Fault; RP = Ronda Peridotite; YF = Yusuf Fault.

complemented by vintage deep-penetration reprocessed MCS profiles. The main objectives of this work are (i) to characterize the crustal types within the Alboran Basin, (ii) to interpret the nature of the basement types on the basis of seismic images and available basement samples, and (iii) to contextualize the crustal configuration in a geodynamic evolutionary model.

2. Geological Setting

The Gibraltar Arc system resulted from the interaction between the Iberian and African plates, and exotic terrains collectively known as the Alboran Domain (Balanyá & García-Dueñas, 1987; García-Dueñas et al., 1992; Sanz De Galdeano, 1990). The Alboran Domain is formed by three polymetamorphic terrains, in ascending order, the Nevado-Filabride, Alpujarride, and Malaguide complexes (e.g., Sanz de Galdeano,

1990). Recent studies support that the Nevado-Filabride is not part of the Alboran Domain sensu strictu, being mostly the Paleozoic basement of Iberia (Booth-Rea et al., 2015). The evolution of the region containing the Alboran Basin (Figure 1) has been proposed as related to the evolution of a subduction system. A combination of slab roll-back and slab tearing (Lonergan & White, 1997; Spakman & Wortel, 2004; Wortel & Spakman, 2000) has probably driven the entire system affecting the subsidence patterns of parts of the basin (Do Couto et al., 2016), magmatic activity that led to the generation of new basements during the Tortonian (Booth-Rea et al., 2007; Duggen et al., 2004, 2005; Hoernle et al., 1999), and tectonic processes.

The Alboran Basin was mainly formed during the Miocene (Comas et al., 1999; Do Couto et al., 2016; Martínez-García et al., 2017). The extension was accompanied by crustal contamination by magmatism and several volcanic episodes (e.g., Duggen et al., 2004, 2008; Hoernle et al., 1999). The first volcanic episode was late Oligocene to earliest Miocene tholeiitic dykes exposed onshore (Duggen et al., 2004; Marchesi et al., 2012; Torres-Roldan et al., 1986). The second episode occurred during the Late Serravallian-Tortonian, with the emplacement of calk-alkaline, tholeiitic, and shoshonitic volcanics, subduction related, in most of the basin (Duggen et al., 2008). Finally, evidence of a third volcanic episode during the Messinian and Plio-Quaternary is found at the basin margins, where alkaline volcanic rock complexes are probably related to a hot asthenosphere source, rather than subduction-related fluids (Duggen et al., 2004, 2008). During the Late Miocene contractive deformation occurs during the latemost Tortonian in the easternmost section of the system, both onshore (eastern Betics, Booth-Rea et al., 2004) and offshore in the NE margin of Palomares (offshore SE Iberia, Giaconia et al., 2015), whereas much of the basin was under extension. After Messinian time the entire Alboran region undergoes contractive deformation that is clearly active since the Early Pliocene to today (Giaconia et al., 2015; Martínez-García et al., 2013, 2017). The Moho and crustal structure has been mapped onshore (e.g., Díaz et al., 2016; Mancilla & Diaz, 2015), but the offshore crustal structure is comparatively poorly known, with limited resolution velocity models from passive-source data (Grevemeyer et al., 2015). Moho depth (crustal thickness) in the Gibraltar Arc system is very variable, ranging from ~8 km in the Algero-Balearic Basin (ABB) to ~55 km below NW Morocco, at the Rif belt (Díaz et al., 2016). Below the western Betics (South Iberia), the Moho occurs at 40–50 km depth, thinning to ~20 km toward the easternmost Betics, probably related to slab delamination (Mancilla et al., 2015). Similarly, Moho depth under the Rif belt (NW Morocco) is 40–55 km deep, while in NE Morocco and NW Algeria is 25–35 km deep (Díaz et al., 2016; Mancilla & Diaz, 2015). The boundary between these two areas is defined onshore by the Nekor Fault that extends offshore along the Al-Idrissi Fault System. These differing crustal structures are probably related to the Neogene evolution of the subduction system and delamination processes currently affecting this area (e.g., Fadil et al., 2006; Mancilla et al., 2015; Seber et al., 1996). Offshore, the Moho topography has not been resolved in detail. Tomographic models (e.g., Mancilla & Diaz, 2015; Palomeras et al., 2017) do not have enough resolution to image intrabasin thickness variations, mainly due to the lack of offshore stations (Mancilla & Diaz, 2015) and the coarse grid spacing used (~60 × 60 km, Mancilla & Diaz, 2015; Palomeras et al., 2017). These models provided a mean crustal thickness of ~17 km (Palomeras et al., 2017). Local earthquake data record of a temporal network covering the Alboran Basin supports a mean crustal thickness of ~20 km (Grevemeyer et al., 2015).

3. Data and Methods

3.1. Data Acquisition and Processing

The main data set used for this study are MCS data, corresponding to ~2,550 km of the TOPOMED-GASSIS and ~300 km of EVENT-DEEP Leg 2 surveys acquired and processed by our group of the Barcelona CSI. We have also reprocessed ~90 km of vintage data from the ESCI Alboran survey (the ESCI-Alb1 profile, Comas et al., 1995) and integrated the ESCI Alboran lines 2b and 2c and ~990 km of CONRAD cruise data (Figure 1). The MCS profiles from the TOPOMED cruise (October 2011) were acquired on board of the Spanish RV "Sarmiento de Gamboa," using a 5,100 (leg 1) to 6,000 (leg 2) meter long active section of a solid state Sentinel SERCEL streamer with 408 (profiles TM01–TM25) and 480 (profiles TM26–TM30) active sections (12.5 m channel interval), towed at 10 m depth, with compasses every 150 m. The air gun source was 50.15 l (3,060 c.i.). The source array was composed by 8 G-GUN II guns deployed at 7.5/9 m depth, in single

cluster configuration. The air guns were fired every 30 m (profiles TM01 and TM02), 40 m (profiles TM03 to TM05), and 50 m (profiles TM06 to TM31) at a pressure of 2,000 to 2,500 psi. The record length was 14 to 19 s at of 2-ms sampling rate. Profiles from EVENT-DEEP Leg 2 were acquired in June 2010 on board the RV "Sarmiento de Gamboa," using a 3,400-m-long solid state Sentinel SERCEL streamer with 276 channels, 12.5 m long, and a seismic array of 10 air guns, with a total volume of 1,880 c.i. shot every 37.5 m, recording 12 s at 2-ms sampling rate. The ESCI Alboran survey was carried out on board Seismic Vessel "Bin Hai" from WesternGeco (Geco at the time) in February 1992. An air gun array of 7,118 c.i. (2,000 psi) was fired every 75 m, with the signal recorded for 22 s at 4-ms sampling rate, on a 4,500-m-long (180 channels with 25 m group interval) analogue streamer.

TOPOMED, EVENT-DEEP Leg 2, and ESCI profiles have been processed using GLOBE Claritas software. The processing flow was designed to obtain crustal-scale information, preserving resolution in the sedimentary basins, but imaging the deeper parts of the crust. Processing steps in time domain include minimum-phase conversion, streamer geometry definition accounting for feathering, common midpoint sorting, spherical divergence correction, predictive deconvolution in Tau-P domain (to eliminate the bubble and short periods multiple reverberations), surface consistent deconvolution, surface-related multiple elimination, Radon filter demultiple, normal-move-out correction based on velocity semblance analysis, dip move out correction, stretch mute, amplitude recovery, stack, finite differences time migration, and time and spatial variant band-pass filter (for further information about the processing flow, see the supporting information and Figure S4; see also Yilmaz, 1987).

The CONRAD survey carried out in October 1988 on board the RV "Robert D. Conrad" used a BOLT air gun array of 5,346 c.i. fired every ~50 m and a DIGICON 2,400-m-long streamer with 48 active groups spaced 50 m. CONRAD data set was obtained from the Academic Seismic Portal of the University of Texas (UTIG). The available stacks were processed further including statistical deconvolution, time and space variant band-pass filter, amplitude balance, and finite differences time migration.

We used the IHS Kingdom Advanced software to interpret the stratigraphy and the main structures of the MCS data set integrating our multibeam bathymetry compilation (e.g., Ballesteros et al., 2008; Gràcia et al., 2006, 2012) and used Generic Mapping Tools (Wessel & Smith, 1991) to plot seismic images. Seafloor map analysis and display were done with ArcGIS software.

3.2. Moho Interpretation

Since the 1980s, several studies demonstrated the feasibility to use MCS records to characterize crustal structures. Different national projects like DEKORP (Deutsches Kontinentales Reflexionsseismisches Programm, Meissner et al., 1983), BIRPS (The British Institutions Reflection Profiling Syndicate, Klemperer & Matthews, 1987; Matthews, 1982), or COCORP (Consortium for Continental Reflection Profiling, Allmendinger et al., 1983) and international projects like BABEL (Baltic and Bothnian Echoes from the Lithosphere, BABEL working Group, 1993) and IAM (Iberian Atlantic Margins, Dean et al., 2000) collected land and marine seismic reflection records that imaged the entire crust at the time, with unprecedented vertical and horizontal resolution.

In wide-angle seismic data, the crust-mantle or Moho boundary is associated with an abrupt increase in seismic velocities. In coincident multichannel reflection seismic profiles, this velocity step correlates either with a sharp reflection or with the base of the more or less reflective lower crust, which not always correspond to the location of the brightest reflections (e.g., BABEL working group, 1993; Freeman et al., 1988; Knapp et al., 1996). Reflectivity in the upper mantle has rarely been imaged and typically occurs as discrete events striking with an angle to the crustal structure. Their origin is uncertain and widely debated (BABEL working group, 1993).

Some of these studies report a discontinuous and laminated character for the Moho reflection, while it exhibits a sharp discontinuous character on velocity models obtained from coincident wide-angle seismic profiles. This difference has been associated with the finest resolution obtained by reflection data at the complex transition zone between the crust and the mantle (Hale & Thompson, 1982). Recent models testing how a 3-D deep laminated zone is imaged in 2-D supports that destructive interferences destroy part of the reflected signal (Hobbs et al., 2006). Thus, a weak signal is not necessarily indicative of a gradational Moho boundary.

Following previous studies, we have interpreted the Moho boundary as the deepest continuous clear reflection or as the base of the more dispersed reflectivity. We have detected the Moho boundary along all seismic lines. Although the Moho signal changes in strength among the sections, a seismic boundary can be correlated across the entire basin, supporting a consistency in our interpretation. The events located above the base of the reflectivity have been interpreted as intracrustal features, discussed in section 5.1.

4. Reflective Character of the Crust

The deep penetration seismic images display five different domains with different types of crustal reflectivity: the West Alboran Basin (WAB), the Malaga Basin (MB), the East Alboran Basin (EAB), the North African margin (NAM), and the transition to the ABB. The domains with different crustal types are defined using well sites and dredge information, providing—locally—the nature of the basement.

4.1. The WAB

The WAB is a deep sedimentary depocenter, with ~6–7 s TWTT of infill (~7–8 km thick) accumulated since the Late Aquitanian-Burdigalian (~21 Ma, Do Couto et al., 2016), with a sequence with no tectonic deformation (Figures 1 and 2a). Metamorphic basement similar to Alboran Domain on-land was drilled during DSDP Leg 121 and ODP Leg 161 (Comas et al., 1992, 1999). These metamorphic rocks are dated Late Oligocene-Early Miocene (~27–19 Ma, Comas et al., 1999; Kelley & Platt, 1999). At the south eastern side of the WAB, volcanic intrusions occur (Duggen et al., 2004).

The metamorphic basement has low internal reflectivity (Figures 2a, 3a, and 4a). The basement top is a bright reflection at highs (Figure 2a, common midpoints (CMPs) 16000–14000) and indistinct under the deep basin, where it is inferred at the base of continuous parallel reflections interpreted as sediments (Figure 3a, CMPs 19000–16000). The Moho boundary is delineated by faint discontinuous reflections (e.g., Figures 2a, 3a, and 4) with slightly higher amplitude than the background reflectivity (e.g., Figures 2 and 4). Discrete reflections locally occur in the uppermost mantle (Figure 3a).

The basement top occurs at 5–8 s TWTT under the basin depocenter (Figures 2a, CMPs 20000–16000, and 4a, CMPs 2000–8000) and rises toward a high at ~2 s TWTT sampled by ODP and DSDP drilling expeditions (Figures 2a, CMPs 16000–10000 and Figure 4a, CMPs 8000–10000). The Moho occurs at 7–8 s TWTT in the northern sector (Figure 2a, CMPs 20000–16000) and at 8–10 s TWTT on the southwestern sector (Figure 4a, CMPs 2000–10000). Underneath the basement highs, the Moho is not well defined, although indistinct events occur at ~8 s TWTT (Figure 2a, CMP ~14000, ~12000). At the center of the basin basement thickness is only ~1–2.5 s TWTT (~4–6 km, Figures 2a, CMPs 20000–17000, Figure 4a, CMPs 2000–7000). In the basement highs, basement thickness is ~ 5 s TWTT (Figures 2a and 2b, CMPs 16000–8000, Figure 4a, CMPs 7000–11000). Approaching the Straits of Gibraltar, the Moho occurs at ~8 s TWTT and basement thickens to ~6–7 s TWTT. The southeastern sector contains volcanic highs cropping out at the seafloor (Figures 1 and 2b) indicating that metamorphic basement has been affected by magmatic arc activity (Figure 2b).

4.2. The MB

The MB depocenter is $>$6 s TWTT deep and drilling of basement on its northern flank recovered metamorphic samples (Figure 1, Andalucia A-1, Comas et al., 1992), sharing similarities to the WAB basement.

Under the MB, the top of the basement is poorly defined, and it is inferred at the base of a set of subhorizontal continuous reflections (Figure 5). The basement shows two layers, with different reflectivity: the upper crust that shows poor reflectivity, while the lower crust is characterized by higher reflectivity (Figure 3b). The boundary between the upper and lower crust is defined by relatively continuous 5- to 10-km-long groups of high-amplitude reflections with a layered aspect (Figure 3b) that progressively becomes indistinct toward the west and disappears under the WAB (Figure 4b). The Moho reflection character is similar to the WAB, with sparse reflections (Figure 3b) that gain in continuity toward the east, characterized by moderate amplitudes and low frequency (Figure 5a, CMPs 6000–10000 and Figure 5b, CMPs 12000–18000).

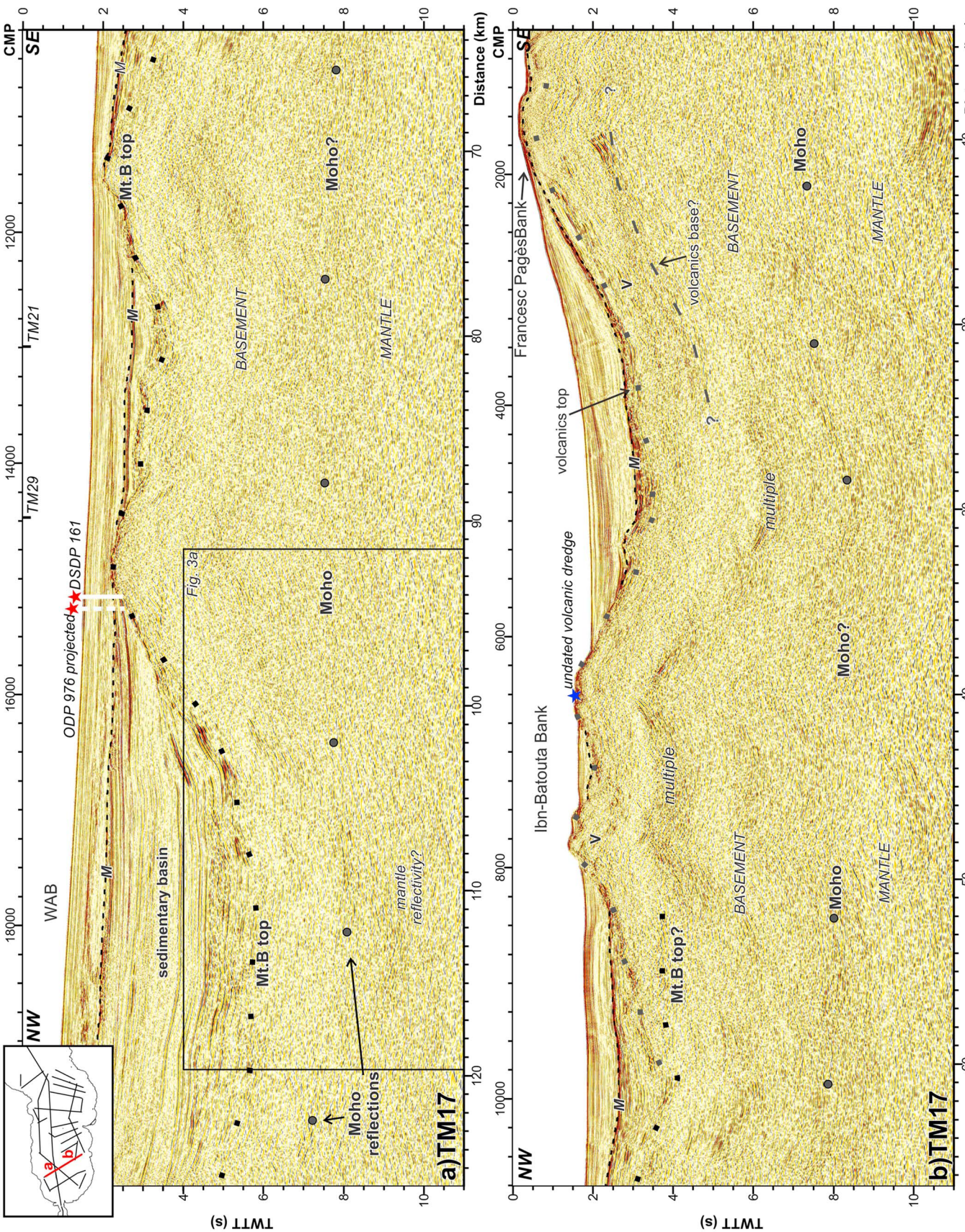

Figure 2. Time migration of profile TM17 (see location in Figure 1). This profile is divided into (a) northern section and (b) southern section. Crustal structure is displayed. M = Messinian top (~5.33 Ma); Mt.B = metamorphic basement; VB = volcanic basement; V = volcanic constructions. Vertical exaggeration is of ~x:1 taking into account basement velocities (~4,500 m/s).

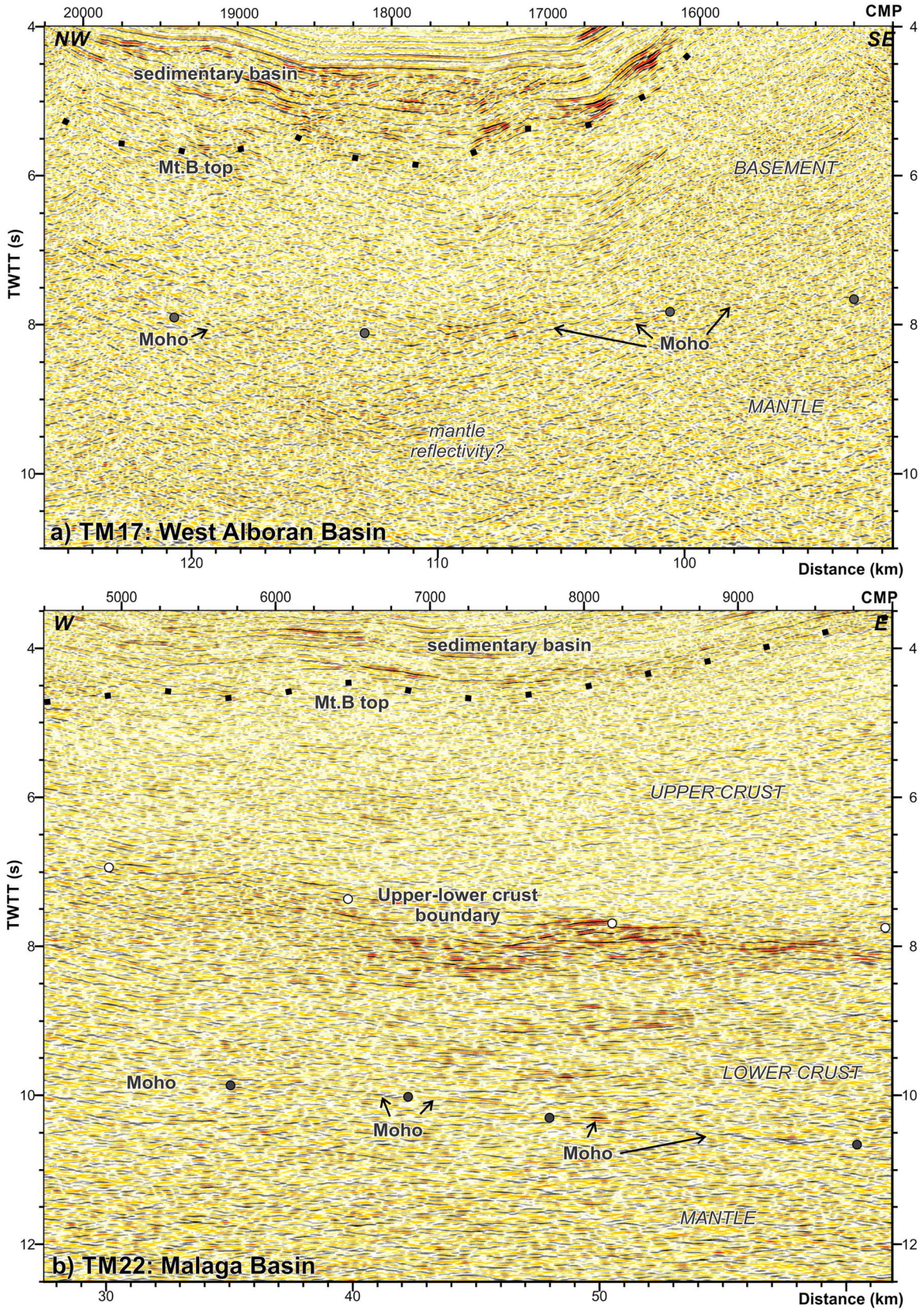

Figure 3. (a) Zoom of profile TM17 (West Alboran Basin). See Figures 1 and 2a for location. (b) Zoom of profile TM22 (Malaga Basin). See Figures 1 and 5a for location. Vertical exaggeration is of ~*x*:1 taking into account deep crust velocities (~6,000 m/s).

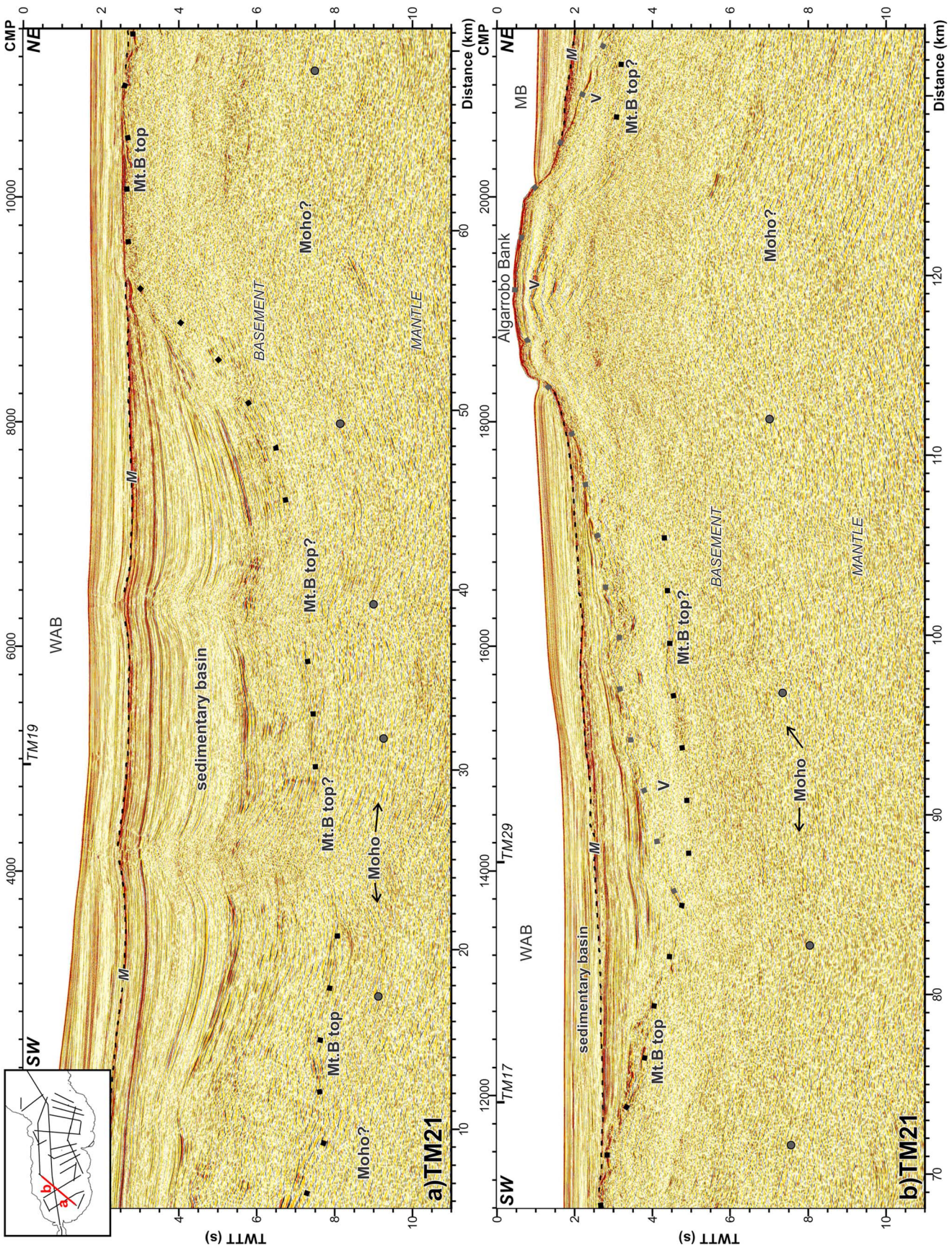

Figure 4. Time migration of profile TM21 (see location in Figure 1). This profile is divided into (a) southwestern section and (b) northeastern section. Crustal structure is displayed. M = Messinian top (~5.33 Ma); Mt.B = metamorphic basement; VB = volcanic basement; V = volcanic constructions. Vertical exaggeration is of ~x:1 taking into account basement velocities (~4,500 m/s).

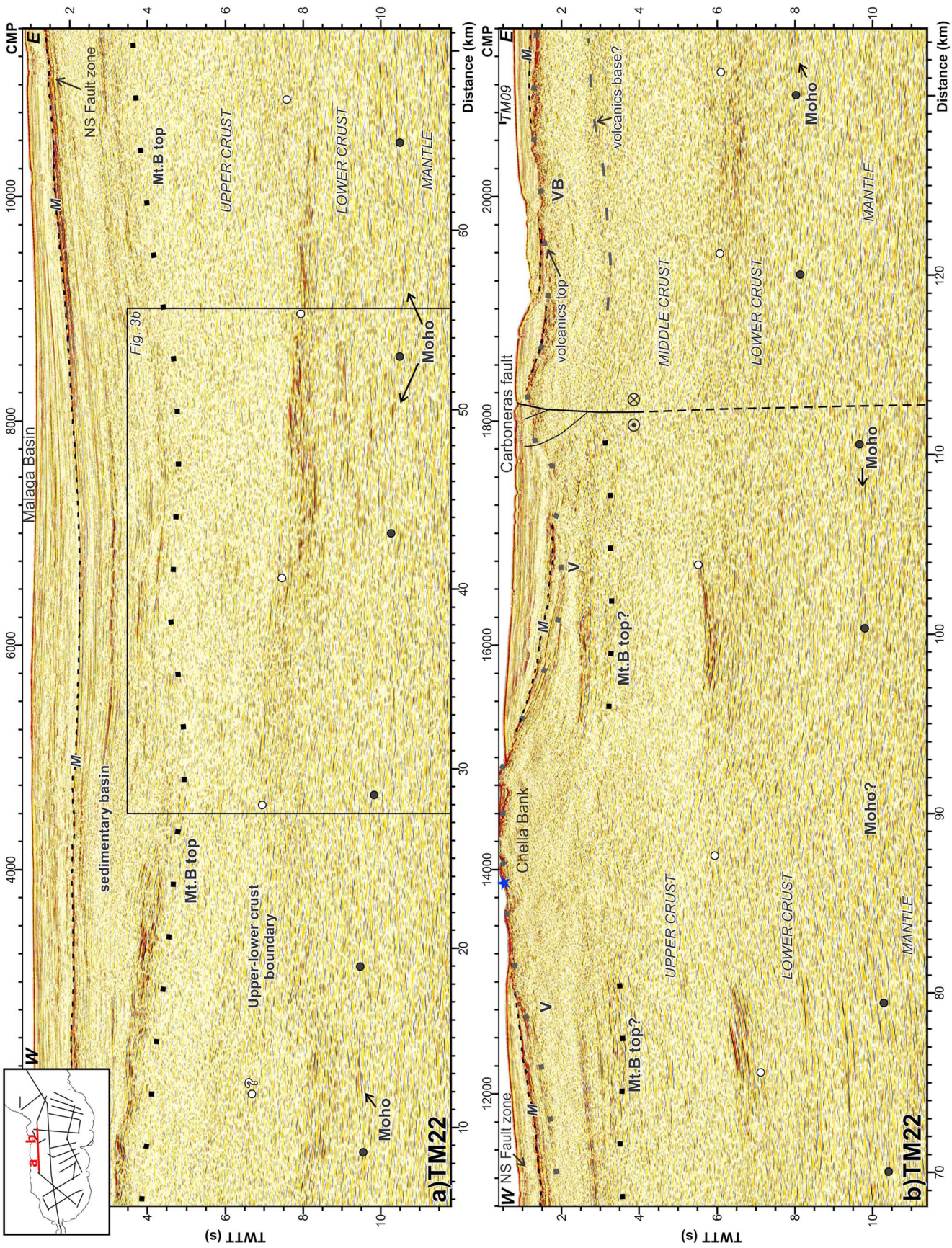

Figure 5. Time migration of profile TM22 (see location in Figure 1). This profile is divided into (a) western section and (b) eastern section. Crustal structure is displayed. M = Messinian top (~5.33 Ma); Mt.B = metamorphic basement; VB = volcanic basement; V = volcanic constructions. Main structures are identified. Blue star: undated volcanic dredge. Vertical exaggeration is of ~x:1 taking into account basement velocities (~4,500 m/s).

Profile TM21 (Figure 4) images the transition between the WAB and the MB. These two subbasins present continuity in the age of the sedimentary infill (Do Couto et al., 2016) and the nature of the continental basement; however, the basement thickness is different. The basement top of the MB is located at ~3.5–5 s TWTT (Figure 5) and the Moho at ~10 s TWTT (Figure 5), that is, ~6–6.5 s TWTT thick, or about 18–20 km thick (using 6-km/s average basement velocity after wide-angle studies onshore, e.g., Banda et al., 1993). The upper crust is <~4 s TWTT thick and the lower crust <~2.5 s TWTT thick.

The eastern end of the MB is abrupt near the Carboneras Fault System (Figure 5b, CMP ~18000) that marks the boundary with the magmatic basement of the EAB. This fault reactivated an inherited structure formed at the middle Miocene (Giaconia et al., 2014; Rutter et al., 2012; Scotney et al., 2000). However, first evidences of activity in the current transpressional regime initiated in latemost Messinian or earliest Pliocene (Moreno et al., 2016), younger than the early Miocene age of the MB (Do Couto et al., 2016). Volcanic constructions grew during the Late Serravallian to Tortonian in the MB near the boundary with the arc crust of the EAB (e.g., Chella Bank in Figure 5b, CMPs 12000–160000).

4.3. The EAB

Dredges of the EAB basement sampled volcanic units of Late Serravallian-Tortonian age (Duggen et al., 2004, 2005, 2008). The volcanic rocks are calc-alkaline enriched in light rare earth elements and depleted light rare earth element tholeites indicating subduction-related melts intruding continental crust and primitive volcanic arc, respectively (Duggen et al., 2004).

Seismic images display a volcanic upper basement unit that laterally changes in thickness creating a complex basement topography that locally appears controlled by faults conceivably formed during the arc accretion (Figures 6a, 7, and 8). This upper unit contains short reflections (3–7 km long) forming complex subhorizontal patterns possibly composed by successive volcanic units. The base of the volcanic units is not a sharp boundary, although it can be mapped due to a change in the reflectivity pattern, as the volcanic units show higher reflectivity than the underlying middle crust (Figure 7). The boundary between the middle and lower crusts is defined by a change from comparatively lower to enhanced reflectivity in the lower crust, containing relatively continuous reflections that form bands perpendicular (Figure 7a) and parallel (Figure 7b) to the basin axis, roughly striking W-E. Moho reflections are indistinct and poorly continuous, so that the Moho boundary has been interpreted at the base of the lower-crust reflectivity (Figures 6a and 7).

The upper unit is up to ~1 s TWTT or ~2–2.5 km thick (assuming 5 km/s), the middle unreflective crust is ~2 s TWTT thick (~6 km thick assuming 6 km/s), and the lower crust is ~3 s TWTT thick (~9 km, Figures 6a, 7, and 8). Thus, the crust of the EAB is ~4–8 s TWTT thick (~10–19 km thick).

Evidence of magmatic arc activity within the Alboran Basin occurs between 4°15′W and 1°W (Figure 1, e.g., Duggen et al., 2004). This magmatism may have led to form a new basement during the growth of the arc (Figures 6a and 8a), as in the case of the EAB (Booth-Rea et al., 2007). However, magmatism locally extends into the pre-existing metamorphic basement, where isolated volcanic edifices occur (e.g., Algarrobo Bank in Figure 4b, CMPs 17000–21000, Chella Bank in Figure 5b, CMPs 12000–160000, Comas et al., 1999; Duggen et al., 2008). These volcanic edifices are characterized by high-amplitude wavy reflections that usually form aprons on the flanks of the volcanic constructions (e.g., Ibn-Batouta Bank in Figure 2b, CMPs 10000–4000; Algarrobo Bank in Figure 4b, CMPs 17000–21000; El Sabinar Bank in Figure 6a, CMPs 2500–4000 and Figure 9). Volcanic edifices commonly show a circular seafloor morphology (Figure 1), that is especially evident in the Chella Bank (Figures 9a–9c), with a mean diameter of ~30 km. In areas floored by volcanic basement, volcanic edifices are also found (Figures 9d–9e). In these areas, elongated ridges are more common than conical edifices (Figure 1), with a mean width of 20 km and different lengths, being the Maimonides Seamount the longest one, more than 50-km-long (Maimonides High in Figure 9d; Yusuf Ridge and Al-Mansour Seamount in Figure 9e). They display a layered stratigraphy of volcanoclastic strata.

The southern EAB boundary with the North African continental crust occurs at (a) the location of the Yusuf strike-slip fault system (Figure 6b, CMPs 10000–12000, Figure 8a, CMPs 7000–9000, and Figure 8b CMPs

10.1029/2017TC004946

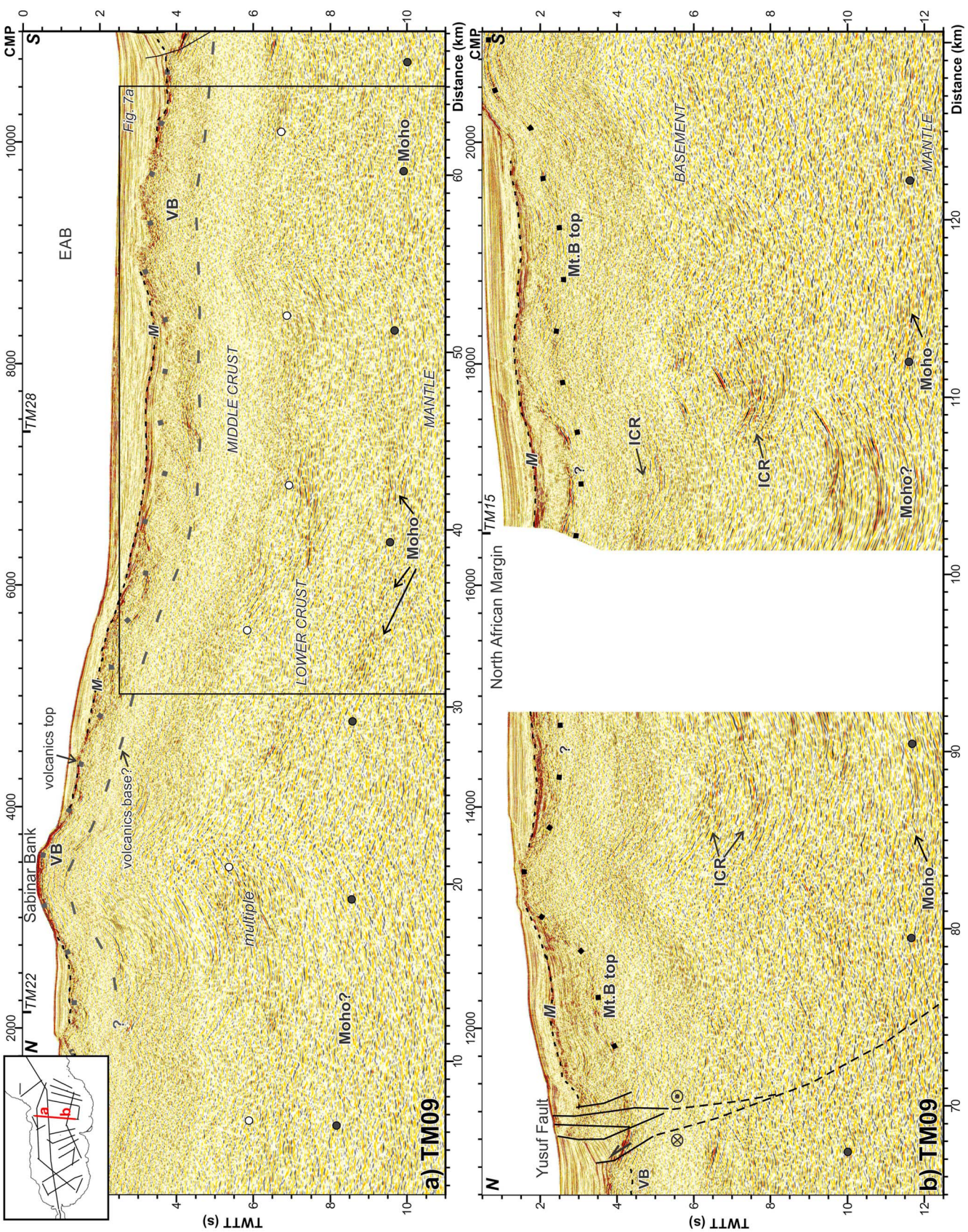

Figure 6. Time migration of profile TM09 (see location in Figure 1). This profile is divided into (a) northern section and (b) southern section. Crustal structure is displayed. M = Messinian top (~5.33 Ma); Mt.B = metamorphic basement; VB = volcanic basement; ICR = intracrustal reflection. Main structures are identified. Vertical exaggeration is of ~x:1 taking into account basement velocities (~4,500 m/s).

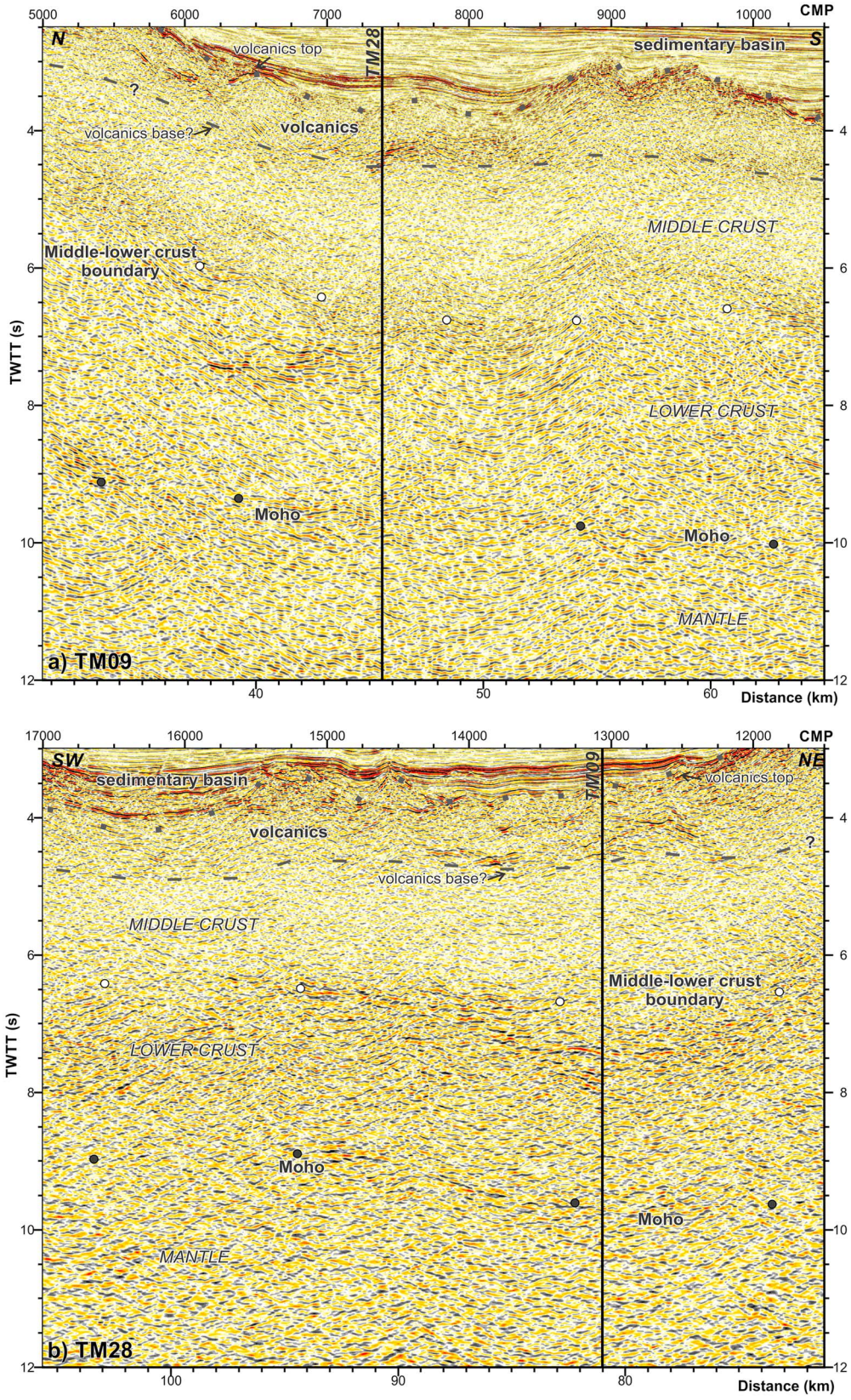

Figure 7. (a) Zoom of profiles TM09 (perpendicular to the margin) and (b) TM28 (parallel to the margin; East Alboran Basin). See Figures 1 and 6a for location. Vertical exaggeration is of ~*x*:1 taking into account deep crust velocities (~6,000 m/s).

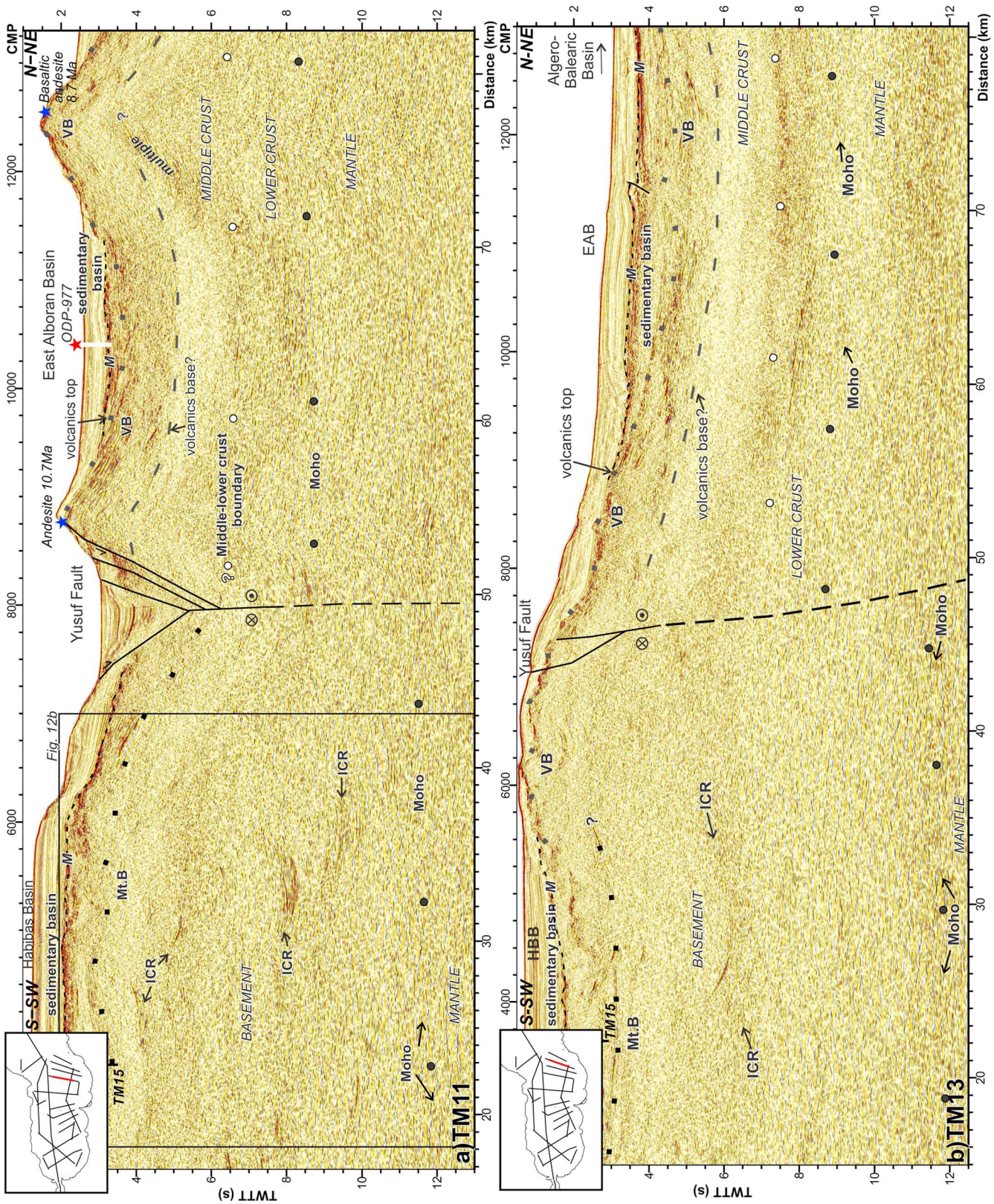

Figure 8. (a) Time migration of profile TM11 (see location in Figure 1). (b) Time migration of profile TM13 (see location in Figure 1). Crustal structure is displayed. Blue stars: volcanic dredges. M = Messinian top (~5.33 Ma); Mt.B = metamorphic basement; VB = volcanic basement; ICR = intracrustal reflection. Vertical exaggeration is of ~*x*:1 taking into account basement velocities (~4,500 m/s).

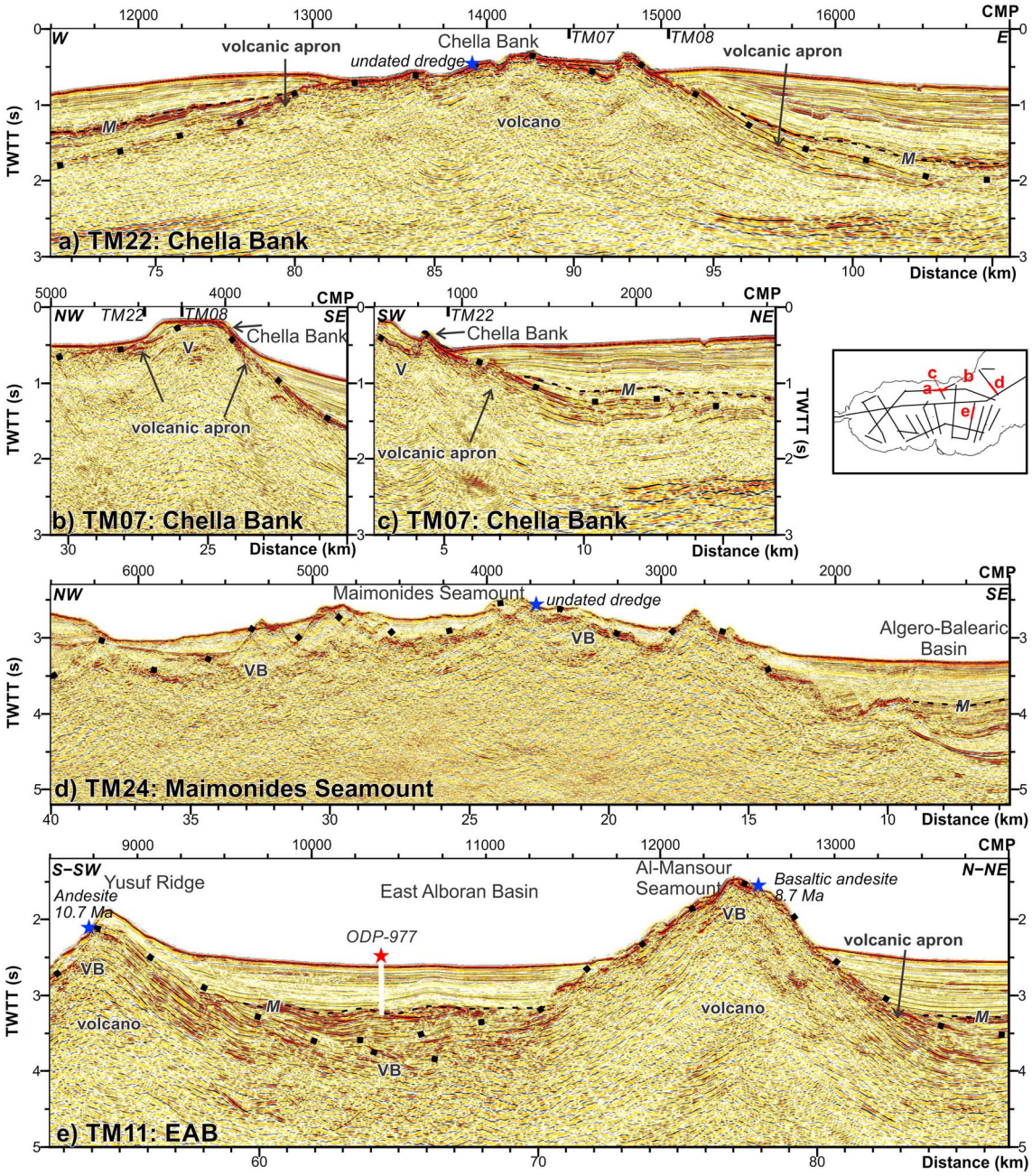

Figure 9. Detail of the volcanic edifices. (a–c) Cross sections of the Chella Bank. Three radial transects are performed, showing an irregular basement top and aprons toward the high flanks. V = volcanic construction. (d) Detailed image of the Maimonides High. An irregular basement top forming conical highs is imaged. VB = volcanic basement. (e) Detail images of the Yusuf Ridge and Al-Mansour volcanic outcrops. Internal wavy reflections developing apron shapes toward the highs flanks are imaged. VB = volcanic basement. Blue stars: volcanic dredges. Vertical exaggeration is of ~x:1.8 taking into account a 3,000-m/s velocity.

7000–8000) and (b) continuous along Alboran Ridge frontal fault system extending westward (Figure 10). Like the Carboneras fault system, Yusuf and Alboran Ridge fault systems are located at the boundary of crustal domains and their fault activity is latemost Messinian or earliest Pliocene (Martínez-García et al., 2013) and thus much younger than the basement age. Toward the east, the volcanic basement of the EAB progressively transitions to the thinner oceanic crust of the ABB (Figure 1, Booth-Rea et al., 2007, 2018).

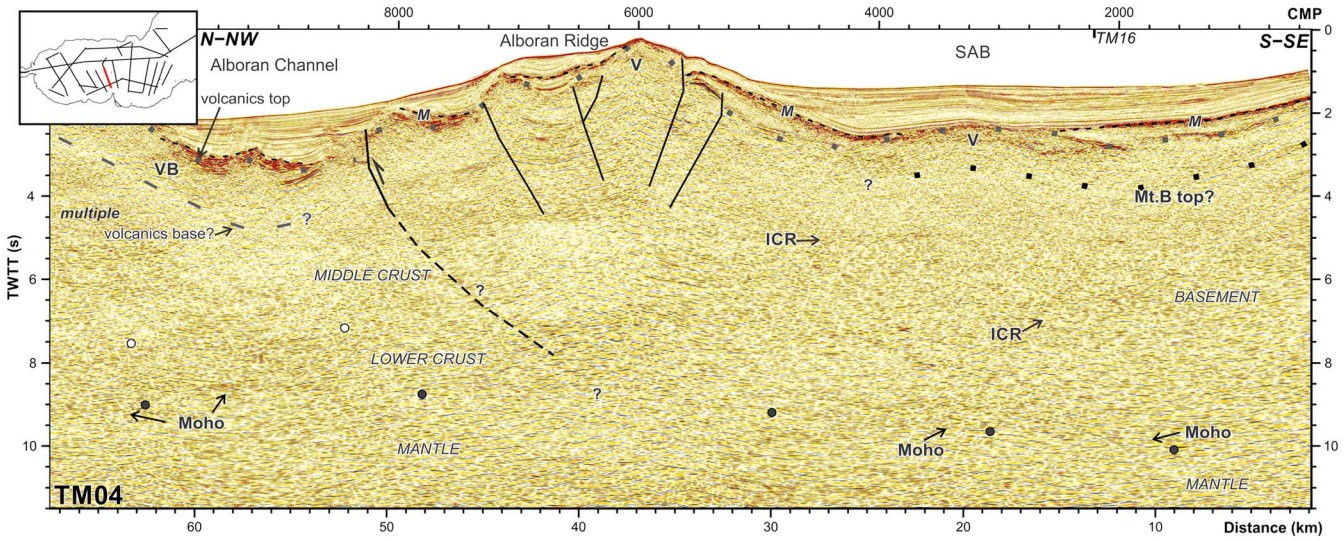

Figure 10. Time migration of profile TM04 (see location in Figure 1). Crustal structure is displayed. M = Messinian top (~5.33 Ma); Mt.B = metamorphic basement; VB = volcanic basement; V = volcanic constructions; ICR = intracrustal reflection. Main structures are identified. Vertical exaggeration is of ~*x*:1 taking into account basement velocities (~4,500 m/s).

4.4. The NAM

The NAM forms the widest shallow water shelf of the Alboran Basin. It contains the Habibas (HBB) and Pytheas (PB) basins (Figure 1), where the HBB-1 well sampled metamorphic basement rocks of possible Late Triassic-Early Jurassic? age (Medaouri et al., 2014). However, a later metamorphic age has been described onshore (Late Oligocene-Middle Miocene, Negro et al., 2007), suggesting that a second metamorphic process affected this margin.

This area is characterized by basement >8.5–10 s TWTT thick (~25–30 km) with comparatively high internal reflectivity where packages of intracrustal reflections (ICRs) are common (Figures 11 and 12). The most continuous ICR packages in the Alboran Basin (5–20 km) occur under the Habibas Basin on images parallel to the margin (Figure 12a) loosing continuity under the Pytheas Basin. The same ICR exhibit much less continuity (2–5 km) on images perpendicular to the margin (Figure 12b). A well-defined boundary between the upper and lower crust is not observed. ICR bands dip toward the NW, and in the lower crust, events stop at a fairly consistent level interpreted as the Moho (Figure 11b), which are better imaged on profiles parallel to the strike of the margin (Figure 12).

Under the Habibas Basin, basement top is interpreted at the base of a synform filled by discontinuous layering inferred to be the oldest infill, underlying well-stratified younger strata (e.g., Figures 11b, CMPs 8000–2000 and 12b). The Moho is interpreted at ~12 s TWTT depth (Figures 11b and 12), shoaling toward the west (Figures 11a and 13).

In the outer western region, the North African basement is affected by magmatic activity (Figures 10, 11a, and 13). South of the Alboran Ridge, the upper unit of the basement under the South Alboran Basin appears made of volcanic layers that locally generate several hundreds of meters of relief. Rhyolites sampled on the Alboran Ridge, yield a Late Serravallian-Tortonian volcanic age (e.g., Duggen et al., 2004; Hoernle et al., 1999). The basement thins from ~10 s TWTT (~30 km) under the Habibas and Pytheas basins to <8 s TWTT under the South Alboran Basin (Figure 10, CMPs 1000–6000, and Figure 13).

4.5. The Transition to the ABB

Under the ABB, the basement top is interpreted at the base of the continuous reflections associated with the sedimentary infill (Figure 14). The basement can be divided into three units: (1) an upper volcanic unit, which base cannot be identified, (2) a middle crust, with lower reflectivity that decreases from top to bottom, and (3)

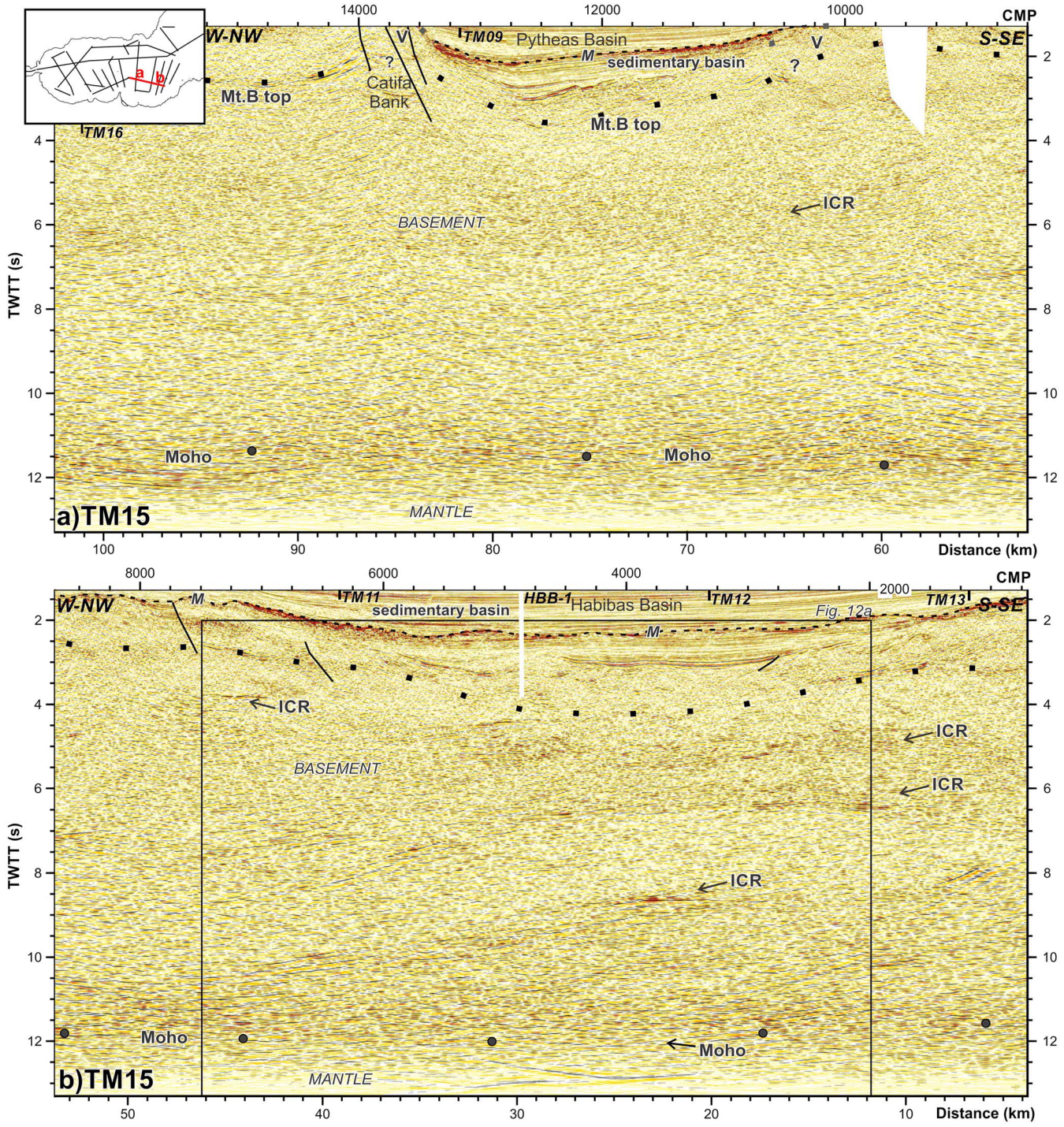

Figure 11. Time migration of profile TM15 (see location in Figure 1). This profile is divided into (a) western section and (b) eastern section. Crustal structure is displayed. M = Messinian top (~5.33 Ma); Mt.B = metamorphic basement; V = volcanic constructions; ICR = intracrustal reflection. Vertical exaggeration is of ~*x*:1 taking into account basement velocities (~4,500 m/s).

a lower crust showing higher reflectivity. The boundary between the middle and the lower crust is defined by a high continuous subhorizontal reflection at ~7–7.5 s TWTT (Figure 14). The Moho is interpreted at the base of the high-reflectivity lower crust, and it is characterized by sparse high-amplitude reflections, <5 km long. The upper volcanic unit and the middle crust are ~1 s TWTT thick (~3 km assuming 6 km/s) and the lower crust is up to ~2 s TWTT thick (~7 km, Figure 14).

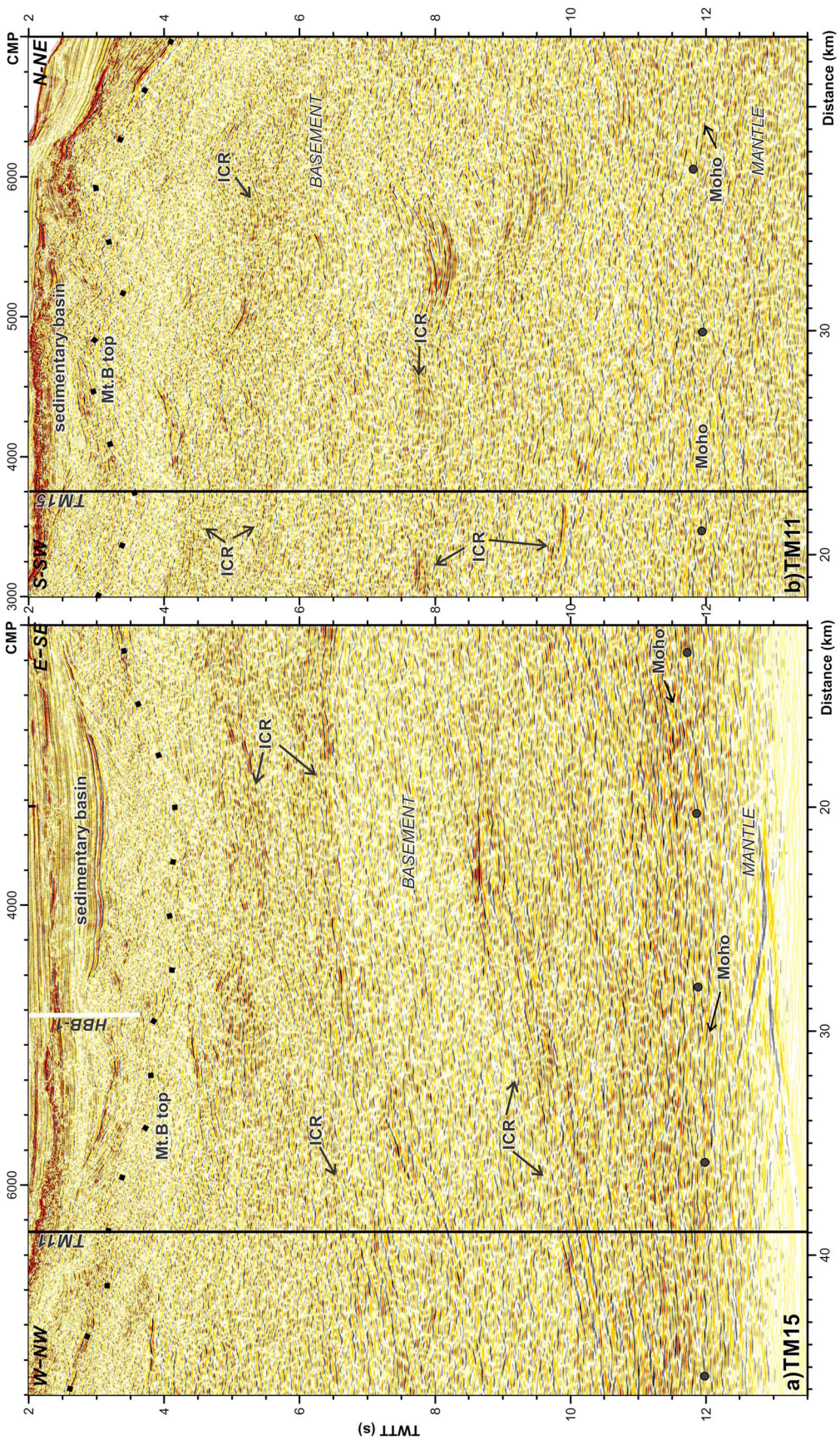

Figure 12. (a) Zoom of profiles TM15 (parallel to the North African margin) and (b) TM11 (perpendicular to the North African margin). See Figures 1, 8a, and 11b for location. Vertical exaggeration is of ~*x*:1 taking into account deep crust velocities (~6,000 m/s).

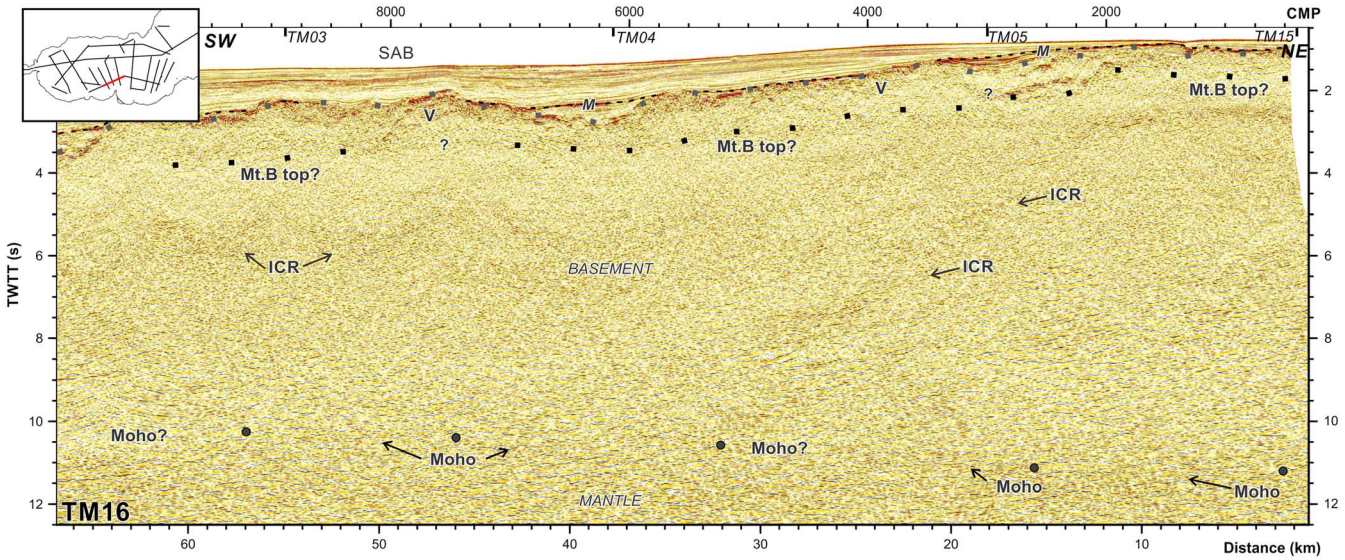

Figure 13. Time migration of profile TM16 (see location in Figure 1). Crustal structure is displayed. M = Messinian top (~5.33 Ma); Mt.B = metamorphic basement; V = volcanic constructions; ICR = intracrustal reflection. Vertical exaggeration is of ~*x*:1 taking into account basement velocities (~4,500 m/s).

5. Discussion

5.1. Nature of the Crustal Domains

Changes in reflectivity and basement internal structure, crustal thickness, and available basement sampling support three main types of crustal domains: (i) relatively thin continental crust under the WAB and MB, and somewhat thicker continental basement under the NAM; (ii) magmatic arc crust of the EAB and NE Alboran Basin (including Mazarron margin); and (iii) a transition to back-arc oceanic crust of the ABB (Figure 15a). The continental crust shows evidence of magmatic constructions in regions adjacent to the magmatic arc-type basement.

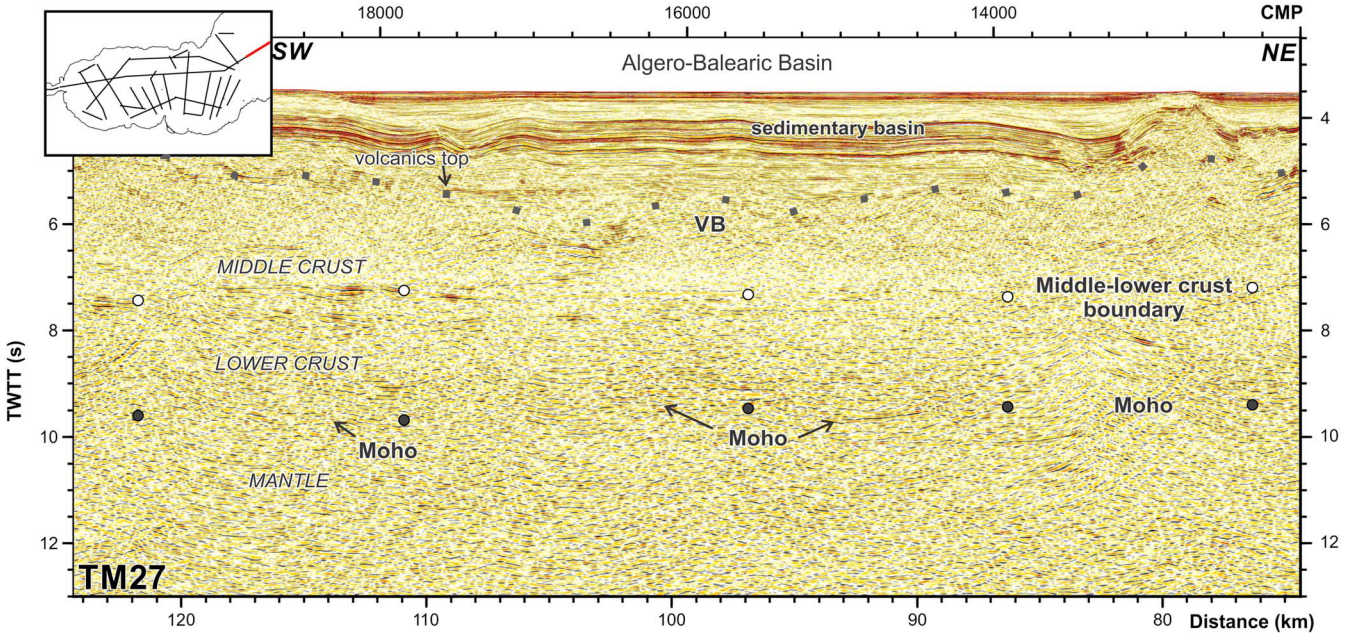

Figure 14. Time migration of profile TM27 (see location in Figure 1). Crustal structure is displayed. VB = volcanic basement. Vertical exaggeration is of ~*x*:1 taking into account basement velocities (~4,500 m/s).

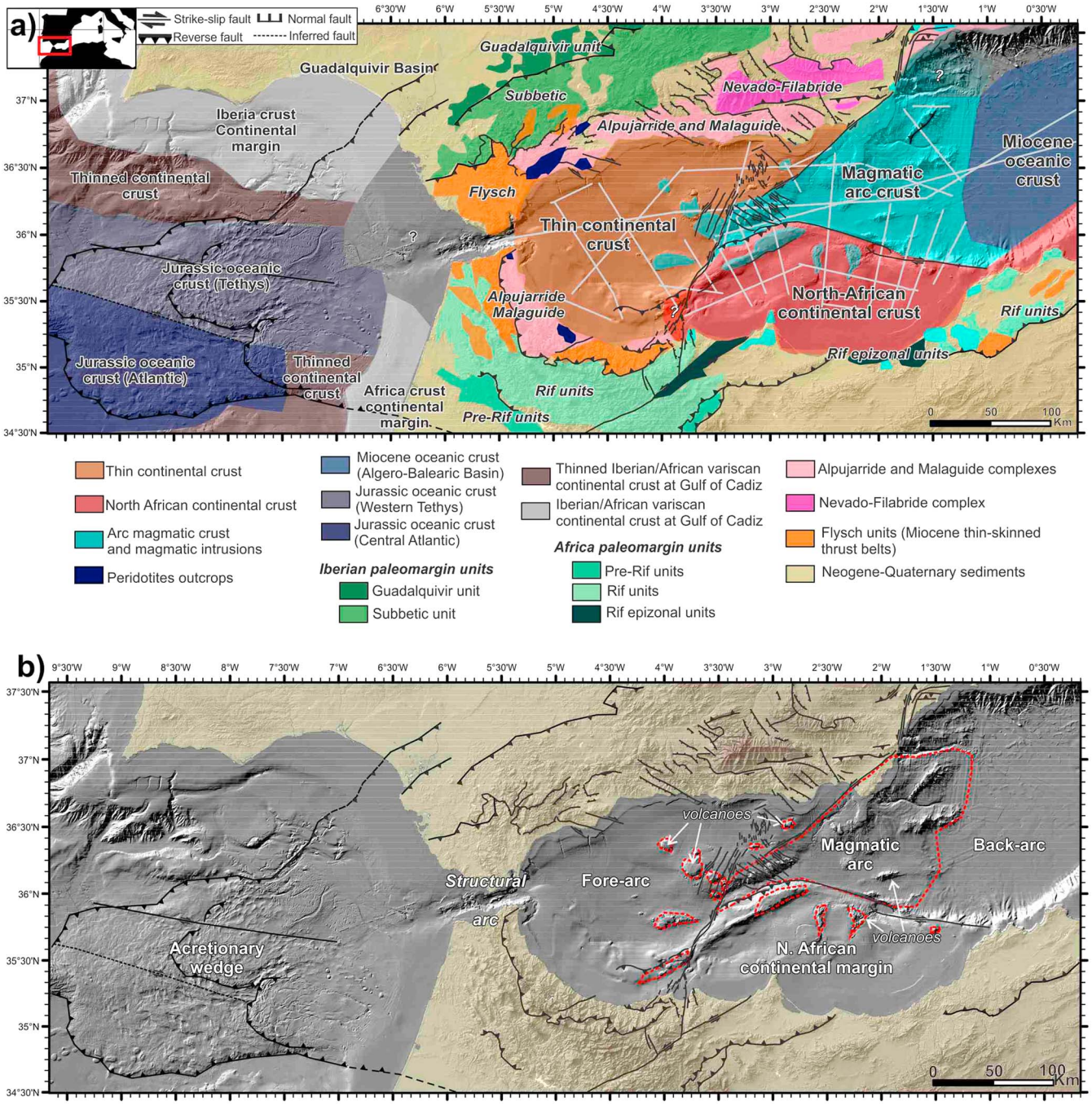

Figure 15. (a) Crustal domains of the Alboran Sea basin. The identified crustal domains are depicted (see figure legend), together with the previous domains identified at the Gulf of Cadiz (Martínez-Loriente et al., 2014) and on-land the Iberian and African margins (from Mancilla et al., 2015). Interpretation of peridotite outcrops is based on Berndt et al. (2014). MCS profiles used in this work are depicted in light gray. (b) Interpretation of the volcanic arc system, divided into fore-arc, magmatic arc, and back-arc basin. Magmatic intrusions and basement of the magmatic arc crust domain are enclosed inside red dashed lines.

5.1.1. Thin Continental Crust Under West Alboran and MBs

We infer a continental nature for the basement of the WAB and the MB on the basis of the metamorphic rocks drilled in DSDP site121, ODP site 976 and industry wells on the Spanish and Moroccan shelfs and the general lack of volcanic constructions and volcanic units as those observed in the magmatic domains. Under the WAB, a faint discontinuous intrabasement seismic event may represent the weakest Moho reflection in the basin, so that the basement is ~2 s TWTT thick (~6 km, Figures 2a and 4). The only basement velocity

information comes from a local earthquake tomography study that seems to support the extension under the basin of the Ronda and Beni Bousera peridotitic massifs cropping out in south Iberia and NW Africa, respectively (El Moudnib et al., 2015). The Ronda Peridotite is overlaid by 5- to 6-km-thin continental crust section (Frasca et al., 2015). Thus, it is conceivable that the basement is made of very thin crust or even of exhumed mantle that is partially serpentinized, so that the faint reflections represent a serpentinization front similar to boundaries observed on the basement of the Iberia Abyssal Plain (Dean et al., 2000). The continental basement thickens toward the E, and to the NE under the MB where clear Moho reflections delineate a ~6 s TWTT thick basement (~18 km, Figure 5a), but the sediment infill and nature of the basement are similar to the basement drilled at the eastern edge of the WAB. In the MB, several volcanic constructions rest on the basement and their volcanoclastic deposits interfinger with the basin infill (Figure 4b, CMPs 18000–21000 and Figure 5a, CMPs 11000–17000).

The thickening of continental basement from the WAB toward the E and NE into the MB indicates that the basement unit underwent different degrees of extension. The higher extension at the WAB produced a deeper depocenter, but in both subbasins thinning is not related to obvious fault activity affecting the basement and the Miocene sedimentary section. However, thinning of a crustal section to fewer than 6 km is accomplished by major faulting with kilometer-scale fault offsets extending over tens of kilometers across the region (e.g., Ranero & Pérez-Gussinyé, 2010). The lack of clear fault-related structures may indicate that it occurred either before the current basin structure formed, or very rapidly during the early sediment deposition, and it is not well displayed on the seismic images. We speculate that thinning, perhaps leading to mantle exhumation (currently onshore and under the WAB) occurred before emplacement of the peridotite massifs in the Early Miocene (~19–22 Ma, Garrido et al., 2011; Hidas et al., 2013; Sosson et al., 1998), thus prior to the early Alboran Basin formation, in Burdigalian times (Frasca et al., 2015). The emplacement of the extended terrane may have obscured the extensional fault structure.

5.1.2. Magmatic Arc-Type Crust in the EAB

The basement of the central and NE regions of the EAB is formed by Neogene magmatism (Booth-Rea et al., 2007, 2018; Giaconia et al., 2015; Gómez de la Peña et al., 2016) sampled in outcrops at the seafloor and onshore in SE Iberia (Duggen et al., 2004, 2005, 2008). The geochemical composition of these volcanic rocks is indicative of subduction-related fluids (Duggen et al., 2004). Basement thickness ranges between 4 s TWTT in the transition to the ABB (~8–10 km) to ~6 s TWTT (~18 km) near the western end of the domain (Figures 6–8) and displays three layers throughout the domain. Across the entire magmatic domain, the volcanic basement is a unit characterized by weakly stratified reflections that, where sampled, are composed by basaltic to andesitic lava flows and ashes (Figure 9e). Below the volcanic layer, comparatively the middle crust is featureless, whereas reflectivity is abundant in the lower crust (Figure 8a, CMPs 9000–12000 and Figure 8b, CMPs 9000–13000). The three-layer structuration and the reflectivity characteristics correlate well with previous studies (Booth-Rea et al., 2007). However, we interpret a slightly deeper Moho under the EAB (~8–10 s TWTT, Figure 6a, CMP 9000–13000, Figure 8a). In contrast to the ESCI lines (Booth-Rea et al., 2007), the processing flow applied to the TOPOMED data included an efficient multiple attenuation (see Figures S4 and S5; see also Monk, 1993; Wang, 2003) that unveils features that otherwise are masked by the multiple energy. In TOPOMED lines, clear reflectivity is observed till ~8–10 s (Figures 7b and 8a, CMPs 9000–13000), supporting our interpretation of the Moho. Lower-crustal reflections display different patterns, with the main two attitudes as subhorizontal events at the top of the lower crust delineating the abrupt transition to a rather transparent middle crust, and at the base of the crust either dipping or subhorizontal. However, the lack of good 3-D control makes it difficult to determine the real attitude of the reflectors. Similar reflections had previously been described on ESCI-Alb line (Figure 1) and interpreted as magmatic layering (Booth-Rea et al., 2007, 2018), which may be the origin of most lower crust reflectivity in the magmatic domain.

All features of this domain are consistent with the arc magmatism interpretation: (i) the volcanic layer made of flows, clasts, and ashes forming the upper crust, as indicated by available basement samples; (ii) the volcanic constructions (Figure 9) with a clear seafloor topography and image of its internal structure are indicative of volcanic edifices (Figures 1 and 9); and (iii) the 8- to 18-km-thick basement with a similar character of lower-crustal reflectivity across the domain.

5.1.3. Continental Crust of the NAM

The continental crust of the NAM has the deepest Moho reflections of the Alboran Basin at ~12 s TWTT, with a basement of ~10 s TWTT or ~30 km thick (Figures 11 and 13). This is slightly thicker than the continental crust

of the North African continental margin facing the ABB that progressively thins from ~25 to ~13 km under the oceanic domain (Aïdi et al., 2018).

Lower crust and Moho reflections are clear in images acquired parallel to the margin trend, with a 1- to 2-s band of reflections apparently dipping to the NW that gently flatten down-dip approaching ~12 s TWTT to give way to a featureless mantle (Figures 11 and 12a). In contrast, images collected perpendicular to the margin trend, display indistinct reflections, with discontinuous lower crustal and Moho reflections (Figures 6b and 8a, CMPs 4000–7000, Figure 8b, CMPs 3000–6000, Figure 12b). Tie points of lines parallel and perpendicular to the margin show that the features creating the conspicuous reflectivity on strike-parallel lines are fairly linear (Figure 12a) with laterally limited extension (Figure 12b). A linear structure in the basement might represent a deformation fabric, like metamorphic mylonites stretching parallel to the margin strike. In contrast, it is rather unlikely that large rock bodies (or compositional layering) of contrasting physical properties produce the lower crustal reflectivity. In particular, the pervasive character of the roughly 1-D seismic fabric supports a tectonic nature of the structure, like mylonitic banding, irrespective of the presence of pre-existing rock bodies with different physical properties. Mylonites have been shown to cause velocity anisotropy capable of creating intrabasement reflectivity (Christensen, 1989; Fountain et al., 1984; Jones & Nur, 1984). This interpretation supports that the continental margin basement may have been sheared, possibly in a ENE-WSW direction, which agrees with the transport direction of extension postulated for the Alboran Basin during the Neogene (e.g., Rosenbaum et al., 2002) and with the mapped mantle anisotropy (Diaz et al., 2010).

The continental basement thins northward toward the EAB as it is progressively affected by magmatic activity indicated by volcanic edifices visible in seismic images and bathymetry (e.g., Figure 13). Magmatic arc intrusions and volcanism heavily modified the basement in the Alboran Ridge area (Duggen et al., 2004, 2008), although magmatism occurred before the uplift of the Alboran Ridge in the Pliocene. The ridge has a basement ~7–8 s TWTT thick (~21–24 km; Figure 13), somewhat thicker than in typical magmatic arc basement nearby, with a reflectivity similar to the basement of Habibas and Pytheas basins. We interpret that this region forms a continental domain, although it has been affected by arc-related volcanism at the edge of the continental margin (Figure 10, CMPs 8000–2000). Transpressive deformation occurred in the Late Oligocene-Middle Miocene (~33–13 Ma, Booth-Rea et al., 2012; Jabaloy-Sánchez et al., 2015; Negro et al., 2008), followed by tectonic denudation during the Late Serravallian-Tortonian (~12–7 Ma, Booth-Rea et al., 2012). This deformation can be explained by strike-slip tectonics affecting the NAM, due to the westward migration of the slab (e.g., van Hinsbergen et al., 2014).

5.2. Crustal Domains Configuration

The characterization of crustal domains of the Gibraltar Arc System onshore have been extensively discussed (e.g., Platt, 2007; Platt et al., 2013; Sanz De Galdeano, 1990). Recent studies with wide-angle and multichannel seismic profiles also constrain the crustal domains on the Gulf of Cadiz area (e.g., Martínez-Loriente et al., 2013; Sallarès et al., 2011, 2013; Sanz De Galdeano, 1990). We integrate in a map of the entire system the crustal domains of the Alboran Basin defined in this work (Figure 15a).

The Gulf of Cadiz is characterized by four main crustal domains that formed during the opening of the Western Tethys and Central Atlantic Oceans, and later during the Neogene subduction of a slab of Tethys lithosphere (Martínez-Loriente et al., 2013; Sallarès et al., 2011, 2013). The Gibraltar Arc System domains onshore are related to the same subduction system, resulting from the collision between allochtonous terrains (Malaguide, Alpujarride, e.g., Balanyá & García-Dueñas, 1987) with the Iberia and Africa margins. The Nevado-Filabride terrain is considered as part of the Iberian basement (e.g., Booth-Rea et al., 2015). The collision led to the formation of the foreland thrust belts, formed by sedimentary rocks of the margins (Rif, Subbetic, and Prebetic units), and the Flysch through units, formed by marine sediments coming from the offscraping from the subducted Tethys ocean slab (Chalouan et al., 2009; Gràcia, Dañobeitia, Vergés, Bartolome, 2003; Luján et al., 2006; Platt et al., 2013; Sanz De Galdeano, 1990). The domains of the Alboran Basin identified in this work appear as an extension of the rock units described onshore. The Ronda and Beni Bousera peridotitic massifs with their thin crustal carapace appear to extend as the 3- to 6-km-thick basement of the domain of the WAB, perhaps containing no crustal basement rocks but serpentinized mantle under the basin depocenter. The continental basement prolongs under the less extended MB. The magmatic

rocks of Cabo de Gata continue as the basement of the Mazarron Margin (Gómez de la Peña et al., 2016) and the magmatic basement of the EAB. The continental rocks along coastal regions of NE Morocco and NW Algeria extend into the North African continental margin.

Limited magmatic activity of late Miocene age reached beyond the boundary between the magmatic arc and continental domains, intruding continental basement, possibly because these were regions of relative thinner lithosphere channeling some melt. Boundaries between the basement domains currently appear to be tectonically reactivated by the largest active tectonic systems offshore: The Carboneras Fault (Figure 5b, CMP 18000), the Yusuf Fault (Figure 8a, CMPs 7000–9000, Figure 8b, CMPs 7000–8000), the Al-Idrissi Fault, and the Alboran Ridge front fault (Figure 10, CMPs 8000–6000) focus on the inherited weakness of boundaries between domains (Figure 15a).

5.3. Geodynamic Setting

On the basis of surface geology or local low-resolution crustal and upper-mantle tomographic studies, different hypotheses were proposed for the origin of the Alboran Basin including orogenic collapse or delamination (e.g., Dewey, 1988; Lonergan & White, 1997; Seber et al., 1996). However, global tomographic models were able to map a slab in the upper mantle, providing an unequivocal link of this system to a subduction system (Spakman & Wortel, 2004) and providing the geodynamic setting to explain Neogene volcanism (Duggen et al., 2004; Hoernle et al., 1999). The distribution of crustal domains across the Alboran Basin described here provides further support to the formation of the Gibraltar Arc System in a subduction setting (Figure 12). The entire Alboran Basin has typically been referred as formed in a back-arc setting, because of its position with respect to structural high formed by the tectonic wedge of the Gibraltar Arc (e.g., Comas et al., 1992). However, the domains can now be placed in a subduction setting and refer them with respect to the volcanic arc and the subduction front: The WAB and MB form the fore-arc basin (Figure 15b); the magmatic arc as originally postulated from geochemical analyses of basement samples (Hoernle et al., 1999) and seismic images (Booth-Rea et al., 2007) extends across the EAB and Mazarron Margin, with large volcanic edifices growing also in the fringes of the continental domains. The actual back-arc basin is found in the ABB. The change in basement type between the volcanic arc and the back-arc oceanic crust is gradual in the seismic images. The volcanic arc images show a complex reflectivity in the crust of 4–6 s TWTT thick (8–18 km; Booth-Rea et al., 2007, 2018 and Figures 5–7), whereas back-arc oceanic crust—that is, formed at the spreading center—is <2–2.5 s TWTT thick (~6–7 km) and exhibits reflections typically restricted to the lower crust (Figure 14), similar to images of oceanic crust from the Pacific (Ranero, Reston, et al., 1997) and the Atlantic (Ranero, Banda, et al., 1997).

The Gulf of Cadiz contains a submarine imbricated sedimentary unit at the front of the subduction system (Figure 15b). However, the lack of a clear trench structure and the proposition that the deformed sediment unit is made of gravity driven deposits (olistostrome) has triggered a debate on its origin that is still open (Gràcia, Dañobeitia, Vergés, Bartolome, 2003; Gutscher et al., 2002; Iribarren et al., 2007; Martínez-Loriente et al., 2013; Torelli et al., 1997). The subduction setting supports that the olistostromic body is the accretionary wedge to the system (e.g., Torelli et al., 1997; Zitellini et al., 2009). The Betics and Rif mountain ranges represent the collisional belt of the system.

6. Conclusions

The analysis of crustal-scale seismic images together with basement samples reveals four different crustal domains forming the basement of the Alboran Basin region: (i) thin continental crust under the WAB and MB, (ii) thicker continental crust under the NAM, (iii) Magmatic arc crust under the EAB and the Mazarron Margin, and (iv) oceanic crust under the ABB.

The thin continental crust ranges from ~1–2.5 s TWTT thickness (~4–6 km) under the WAB to 6–6.5 s TWTT (~18–20 km) under the MB. Under the WAB, the basement is featureless and the Moho is a faint discontinuous reflection with slightly higher amplitude than the background at ~7.5–9 s TWTT depth. Under the MB, the basement is divided into two layers: a low reflectivity upper crust <4 s TWTT thick and a higher reflectivity lower crust <2.5 s TWTT thick. The Moho is defined by a moderate amplitude reflection at ~10 s TWTT depth that gains continuity toward the east. Metamorphic drilled rock samples support the same continental basement nature for both subbasins.

The NAM represents continental basement with up to ~10 s TWTT (~30 km) thickness under much of the continental shelf, thinning toward the north and the west—the domain edges in contact with the volcanic domain. Along the edge, local magmatic intrusions have modified the continental crust. On seismic images, the basement is characterized by a high reflectivity and comparatively abundant ICRs that may represent a mylonitic fabric. The Moho is interpreted at the base of the ICRs at ~12 s TWTT depth, shoaling toward the west.

The magmatic arc crust under the EAB is characterized by ~4–8 s TWTT thickness (~10-~18 km). Based on the reflectivity characteristics, the basement can be divided into three layers: (1) an upper unit <1 s TWTT thick, with high-reflective reflections forming complex patterns and composed by the extrusive volcanic basement; (2) a middle crust ~2 s TWTT thick, characterized by low reflectivity; and (3) a lower crust ~3 s TWTT thickness, exhibiting high-amplitude banded reflections that possibly represent magmatic layering. The Moho is interpreted at the base of the lower crust reflectivity, at ~8–10 s TWTT depth. Several volcanic constructions are found in this area.

The oceanic crust under the ABB is divided into three units: (1) an upper volcanic unit with high amplitude that transitions to (2) a low reflectivity middle-crust, and (3) a lower crust characterized by higher reflectivity and subhorizontal reflections. Total thickness of the crust is ~3–3.5 s TWTT (~9 km). The Moho is at ~9.5 s TWTT depth.

The main active tectonic structures in the present-day compressional setting are located at the boundaries between crustal domains. These boundaries represent the weakest zones in the crust, and thus, they favored fault nucleation and propagation.

The distribution and nature of the crustal domains agrees with the structure expected in a subduction system: a fore-arc basin formed by the WAB and MB, a magmatic arc at the EAB and NE Alboran, and a back-arc basin represented by oceanic crust of the ABB, flanked on either side by continental crust of South-Iberian and NAMs. The northern region of the NAM was deformed possibly by strike-slip tectonics during the Miocene at the southern edge of the subduction system. The Gulf of Cadiz imbricated units are interpreted as the accretionary wedge of the system.

Acknowledgments

The authors acknowledge support from the Spanish Ministry of Economy and Competitiveness through the Complementary Action ESF TopoEurope TOPOMED (CGL2008-03474-E/BTE), national projects EVENT (CGL2006-12861-C02-02), INSIGHT (CTM2015-70155-R), FRAME (CTM-2015-71766-R), and COST Action 1301 "FLOWS." This work was supported by the Spanish Ministry of Education, Culture and Sport through the FPU fellowship 2013–2017 to L. Gómez de la Peña (AP2012-1579). This publication is funded by the Cluster of Excellence "The Future Ocean," within the framework of the Excellence Initiative by the Deutsche Forschungsgemeinschaft (DFG) on behalf of the German federal and state governments. All the data used are listed in the references or archived at the Barcelona-CSI repository at the ICM (TOPOMED, EVENT-DEEP, and ESCI cruises, http://www.icm.csic.es) and at the UTIG repository (CONRAD cruise, http://www.udc.ig.utexas.edu/sdc/).We thank the captain, crew, scientific party, and technicians of the UTM-CSIC on board the Spanish R/V "Sarmiento de Gamboa" during the TOPOMED_Leg 1 cruise. We thank the reviewers whose constructive criticism enabled us to improve our original manuscript. This work has been carried out within Grup de Recerca Consolidat de la Generalitat de Catalunya "Barcelona Center for Subsurface Imaging" (2017 SGR 1662).

References

Aïdi, C., Beslier, M., Yelles-chaouche, A. K., Klingelhoefer, F., Bracene, R., Galve, A., et al. (2018). Deep structure of the continental margin and basin off Greater Kabylia, Algeria—New insights from wide-angle seismic data modeling and multichannel seismic interpretation. *Tectonophysics*, *728–729*, 1–22. https://doi.org/10.1016/j.tecto.2018.01.007

Allmendinger, R. W., Sharp, J. W., Von Tish, D., Serpa, L., Brown, L., Kaufman, S., et al. (1983). Cenozoic and Mesozoic structure of the eastern Basin and Range province, Utah, from COCORP seismic-reflection data. *Geology*, *11*(9), 532. https://doi.org/10.1130/0091-7613(1983)11<532:CAMSOT>2.0.CO;2

BABEL Working Group (1993). Deep seismic reflection/refraction interpretation of crustal structure along BABEL profiles A and B in the southern Baltic Sea. *Geophysical Journal International*, *112*(3), 325–343.

Balanyá & García-Dueñas (1987). Les directions structurales dans le Domaine d'Alborán de part et d'autre du Détroit de Gibralta. *Comptes Rendus Mathematique Academie des Sciences, Paris*, *304*, 929–933.

Ballesteros, M., Rivera, J., Muñoz, A., Muñoz-martín, A., Acosta, J., Carbó, A., & Uchupi, E. (2008). Alboran Basin, southern Spain—Part II: Neogene tectonic implications for the orogenic float model. *Marine and Petroleum Geology*, *25*(1), 75–101. https://doi.org/10.1016/j.marpetgeo.2007.05.004

Banda, E., Gallart, J., García-Dueñas, V., Dañobeitia, J. J., & Makris, J. (1993). Lateral variation of the crust in the Iberian Peninsula: New evidence from the Betic Cordillera. *Tectonophysics*, *221*(1), 53–66. https://doi.org/10.1016/0040-1951(93)90027-H

Berndt, T., Ruiz-Martínez, V. C., & Chalouan, A. (2014). New constraints on the evolution of the Gibraltar Arc from palaeomagnetic data of the Ceuta and Beni Bousera peridotites (Rif, northern Africa). *Journal of Geodynamics*, *84*, 19–39. https://doi.org/10.1016/j.jog.2014.09.014

Bezada, M. J., Humphreys, E. D., Toomey, D. R., Harnafi, M., Dávila, J. M., & Gallart, J. (2013). Evidence for slab rollback in westernmost Mediterranean from improved upper mantle imaging. *Earth and Planetary Science Letters*, *368*, 51–60. https://doi.org/10.1016/j.epsl.2013.02.024

Booth-Rea, G., Azañón, J. M., & García-Dueñas, V. (2004). Extensional tectonics in the northeastern Bethics (SE Spain): Case study of extension in a multilayered upper crust with contrasting rheologies. *Journal of Structural Geology*, *26*(11), 2039–2058. https://doi.org/10.1016/j.jsg.2004.04.005

Booth-Rea, G., Jablaoy-Sánchez, A., Azdimousa, A., Asebriy, L., Váyquey Vílchez, M., & Martínez-Martínez, J. M. (2012). Upper-crustal extension during oblique collision: The Temsamane extensional detachment (eastern Rif, Morocco). *Terra Nova*, *24*(6), 505–512. https://doi.org/10.1111/j.1365-3121.2012.01089.x

Booth-Rea, G., Martínez-Martínez, J. M., & Giaconia, F. (2015). Continental subduction, intracrustal shortening, and coeval upper-crustal extension: P-T evolution of subducted south Iberian paleomargin metapelites (Betics, SE Spain). *Tectonophysics*, *663*, 122–139. https://doi.org/10.1016/j.tecto.2015.08.036

Booth-Rea, G., Ranero, C. R., & Grevemeyer, I. (2018). The Alboran volcanic-arc modulated the Messinian faunal exchange and salinity crisis. *Scientific Reports*, *8*, 13025. https://doi.org/10.1038/s41598-018-31307-7

Booth-Rea, G., Ranero, C. R., Martínez-Martínez, J. M., & Grevemeyer, I. (2007). Crustal types and tertiary tectonic evolution of the Alborán Sea, western Mediterranean. *Geochemistry, Geophysics, Geosystems*, *8*, Q10005. https://doi.org/10.1029/2007GC001639

Chalouan, A., Michard, A., El Kadiri, K., Negro, F., Frizon de Lamotte, D., Soto, J. I., & Saddiqi, O. (2009). The Rif belt. In *Continental evolution: The geology of Morocco. Lecture notes in earth sciences* (Chapter 5, pp. 203–302). Berlin: Springer-Verlat. https://doi.org/10.1007/978-3-540-77076-3_5

Chertova, M. V., Spakman, W., Geenen, T., van den Berg, A. P., & van Hinsbergen, D. J. J. (2014). Underpinning tectonic reconstruction of the western Mediterranean region with dynamic slab evolution from 3-D numerical modeling. *Journal of Geophysical Research: Solid Earth*, *119*, 1119–1144. https://doi.org/10.1002/2013JB010500

Christensen, N. I. (1989). Reflectivity and seismic properties of the deep continental crust. *Journal of Geophysical Research*, *94*, 17,793–17,804. https://doi.org/10.1029/JB094iB12p17793

Comas, M. C., Dañobeitia, J. J., Álvarez-Marrón, J., & Soto, J. I. (1995). Crustal reflections and structure in the Alborán basin: Preliminary results of the ESCI-Alborán survey. *Revista - Sociedad Geológica de España*, *8*(4), 529–542.

Comas, M. C., García-Dueñas, V., & Jurado, M. J. (1992). Neogene tectonic evolution of the Alboran Sea from MCS data. *Basin Evolution*, 157–164.

Comas, M. C., Platt, J. P., Soto, J. I., & Watts, A. B. (1999). 44. The origin and tectonic history of the Alboran Basin: Insights from leg 161 results. *Proceedings of the Ocean Drilling Program, Scientific Results*, *161*, 555–580.

d'Acremont, E., Gutscher, M. A., Rabaute, A., Mercier de Lépinay, B., Lafosse, M., Poort, J., et al. (2014). High-resolution imagery of active faulting offshore Al Hoceima, Northern Morocco. *Tectonophysics*, *632*, 160–166. https://doi.org/10.1016/j.tecto.2014.06.008

Dean, S. M., Minshull, T. A., Whitmarsh, R. B., & Louden, K. E. (2000). Deep structure of the ocean-continent transition in the southern Iberia Abyssal Plain from seismic refraction profiles: The IAM-9 transect at 40°20′N. *Journal of Geophysical Research*, *105*, 5859–5885. https://doi.org/10.1029/1999JB900301

Dewey, J. F. (1988). Extensional collapse of orogens. *Tectonics*, *7*, 1123–1139. https://doi.org/10.1029/TC007i006p01123

Díaz, J., Gallart, J., & Carbonell, R. (2016). Moho topography beneath the Iberian-western Mediterranean region mapped from controlled-source and natural seismicity surveys. *Tectonophysics*, *692*, 74–85. https://doi.org/10.1016/j.tecto.2016.08.023

Diaz, J., Gallart, J., Villaseñor, A., Mancilla, F., Pazos, A., Córdoba, D., et al. (2010). Mantle dynamics beneath the Gibraltar Arc (western Mediterranean) from shear-wave splitting measurements on a dense seismic array. *Geophysical Research Letters*, *37*, L18304. https://doi.org/10.1029/2010GL044201

Do Couto, D., Gorini, C., Jolivet, L., Lebret, N., Augier, R., Gumiaux, C., et al. (2016). Tectonic and stratigraphic evolution of the Western Alboran Sea Basin in the last 25Myrs. *Tectonophysics*, *677-678*, 280–311. https://doi.org/10.1016/j.tecto.2016.03.020

Duggen, S., Hoernle, K., Klügel, A., Geldmacher, J., Thirlwall, M., Hauff, F., et al. (2008). Geochemical zonation of the Miocene Alborán Basin volcanism (westernmost Mediterranean): Geodynamic implications. *Contributions to Mineralogy and Petrology*, *156*(5), 577–593. https://doi.org/10.1007/s00410-008-0302-4

Duggen, S., Hoernle, K., van den Bogaard, P., & Garbe-Schönberg, D. (2005). Post-collisional transition from subduction-to intraplate-type magmatism in the westernmost Mediterranean: Evidence for continental-edge delamination of subcontinental lithosphere. *Journal of Petrology*, *46*(6), 1155–1201. https://doi.org/10.1093/petrology/egi013

Duggen, S., Hoernle, K., van den Bogaard, P., & Harris, C. (2004). Magmatic evolution of the Alboran region: The role of subduction in forming the western Mediterranean and causing the Messinian salinity crisis. *Earth and Planetary Science Letters*, *218*(1–2), 91–108. https://doi.org/10.1016/S0012-821X(03)00632-0

El Moudnib, L., Villaseñor, A., Harnafi, M., Gallart, J., Pazos, A., Serrano, I., et al. (2015). Crustal structure of the Betic-Rif system, western Mediterranean, from local earthquake tomography. *Tectonophysics*, *643*, 94–105. https://doi.org/10.1016/j.tecto.2014.12.015

Fadil, A., Engineering, C., Avenue, I. S., Vernant, P., Mcclusky, S., & Reilinger, R. (2006). Active tectonics of the western Mediterranean: Geodetic evidence for rollback of a delaminated subcontinental lithospheric slab beneath the Rif Mountains, Morocco. *Geology*, *34*(7), 529–532. https://doi.org/10.1130/G22291.1

Fichtner, A., & Villaseñor, A. (2015). Crust and upper mantle of the western Mediterranean—Constraints from full-waveform inversion. *Earth and Planetary Science Letters*, *428*, 52–62. https://doi.org/10.1016/j.epsl.2015.07.038

Fountain, D. M., Hurich, C. A., & Smithson, S. B. (1984). Seismic reflectivity of mylonite zones in the crust. *Geology*, *12*(4), 195–198. https://doi.org/10.1130/0091-7613(1984)12<195:SROMZI>2.0.CO;2

Frasca, G., Gueydan, F., & Brun, J. P. (2015). Structural record of Lower Miocene westward motion of the Alboran Domain in the Western Betics, Spain. *Tectonophysics*, *657*, 1–20. https://doi.org/10.1016/j.tecto.2015.05.017

Freeman, B., Klemperer, S. L., & Hobbs, R. W. (1988). The deep structure of Northern England and the Iapetus suture zone from BIRPS deep seismic reflection profiles. *Journal of the Geological Society, London*, *145*(5), 727–740. https://doi.org/10.1144/gsjgs.145.5.0727

García-Dueñas, V., Balanyá, J. C., & Martínez-Martínez, J. M. (1992). Miocene extensional detachments in the outcropping basement of the northern Alboran Basin (Betics) and their tectonic implications. *Geo-Marine Letters*, *12*(2–3), 88–95. https://doi.org/10.1007/BF02084917

Garrido, C. J., Gueydan, F., Booth-Rea, G., Precigout, J., Hidas, K., Padrón-Navarta, J. A., & Marchesi, C. (2011). Garnet lherzolite and garnet-spinel mylonite in the Ronda peridotite: Vestiges of Oligocene backarc mantle lithospheric extension in the western Mediterranean. *Geology*, *39*(10), 927–930. https://doi.org/10.1130/G31760.1

Giaconia, F., Booth-Rea, G., Martínez-Martínez, J. M., Azañõn, J. M., Storti, F., & Artoni, A. (2014). Heterogeneous extension and the role of transfer faults in the development of the southeastern Betic basins (SE Spain). *Tectonics*, *33*, 2467–2489. https://doi.org/10.1002/2014TC003681

Giaconia, F., Booth-Rea, G., Ranero, C. R., Gràcia, E., Bartolome, R., Calahorrano, A., et al. (2015). Compressional tectonic inversion of the Algero-Balearic basin: Latemost Miocene to present oblique convergence at the Palomares margin (western Mediterranean). *Tectonics*, *34*, 1516–1543. https://doi.org/10.1002/2015TC003861

Gómez de la Peña, L., Gràcia, E., Muñoz, A., Acosta, J., Gómez-Ballesteros, M., Ranero, C. R., & Uchupi, E. (2016). Geomorphology and Neogene tectonic evolution of the Palomares continental margin (western Mediterranean). *Tectonophysics*, *689*, 25–39. https://doi.org/10.1016/j.tecto.2016.03.009

Gràcia, E., Bartolome, R., Lo Iacono, C., Moreno, X., Stich, D., Martínez-Diaz, J. J., et al. (2012). Acoustic and seismic imaging of the Adra Fault (NE Alboran Sea): In search of the source of the 1910 Adra earthquake. *Natural Hazards and Earth System Sciences*, *12*(11), 3255–3267. https://doi.org/10.5194/nhess-12-3255-2012

Gràcia, E., Dañobeitia, J., Vergés, J., & Bartolome, R. (2003). Crustal architecture & tectonic evolution of the Gulf of Cadiz (SW Iberian margin) at the convergence of the Eurasian & African Plates. *Tectonics*, *22*(4), 1033. https://doi.org/10.1029/2001TC901045

Gràcia, E., Dañobeitia, J. J., Vergés, J., & Parsifal Team (2003). Mapping active faults offshore Portugal (38°N-36°N): Implications for seismic hazard assessment along the southwest Iberian margin. *Geology*, *31*(1), 83–86. https://doi.org/10.1130/0091-7613(2003)031<0083:MAFOPN>2.0.CO;2

Gràcia, E., Pallàs, R., Soto, J. I., Comas, M., Moreno, X., Masana, E., et al. (2006). Active faulting offshore SE Spain (Alboran Sea): Implications for earthquake hazard assessment in the Southern Iberian margin. *Earth and Planetary Science Letters*, *241*(3–4), 734–749. https://doi.org/10.1016/j.epsl.2005.11.009

Grevemeyer, I., Gràcia, E., Villaseñor, A., Leuchters, W., & Watts, A. B. (2015). Seismicity and active tectonics in the Alboran Sea, western Mediterranean: Constraints from an offshore-onshore seismological network and swath bathymetry data. *Journal of Geophysical Research: Solid Earth*, *121*, 767–787. https://doi.org/10.1002/2015JB012352

Gutscher, M. A., Malod, J., Rehault, J. P., Contrucci, I., Klingelhoefer, F., Mendes-Victor, L., & Spakman, W. (2002). Evidence for active subduction beneath Gibraltar. *Geology*, *30*(12), 1071–1074. https://doi.org/10.1130/0091-7613(2002)030<1071:EFASBG>2.0.CO;2

Hale, L. D., & Thompson, G. A. (1982). Mohorovicic discontinuity. *Journal of Geophysical Research*, *87*, 4625–4635. https://doi.org/10.1029/JB087iB06p04625

Hidas, K., Booth-rea, G., Garrido, C. J., Martínez-Martínez, J. M., Padrón-Navarta, J. A., Konc, Z., et al. (2013). Backarc basin inversion and subcontinental mantle emplacement in the crust: Kilometre-scale folding and shearing at the base of the proto-Alborán lithospheric mantle (Betic Cordillera, southern Spain). *Journal of the Geological Society*, *170*, 47–55. https://doi.org/10.1144/jgs2011-151

Hobbs, R. W., Drummond, B. J., & Goleby, B. R. (2006). The effects of three-dimensional structure on two-dimensional images of crustal seismic sections and on the interpretation of shear zone morphology. *Geophysical Journal International*, *164*(3), 490–500. https://doi.org/10.1111/j.1365-246X.2006.02814.x

Hoernle, K., van den Bogaard, P., Duggen, S., Mocek, B., & Garbe-Schönberg, D. (1999). Evidence for Miocene subduction beneath the Alboran Sea: 40Ar/39Ar dating and geochemistry of volcanic rocks from Holes 977A and 978A. *Proceedings of the Ocean Drilling Program*. https://doi.org/10.2973/odp.proc.sr.161.264.1999

Iribarren, L., Vergés, J., Camurri, F., Fullea, J., & Fernández, M. (2007). The structure of the Atlantic-Mediterranean transition zone from the Alboran Sea to the Horseshoe Abyssal Plain (Iberia-Africa plate boundary). *Marine Geology*, *243*(1–4), 97–119. https://doi.org/10.1016/j.margeo.2007.05.011

Jabaloy-Sánchez, A., Azdimousa, A., Booth-rea, G., Asebriy, L., Vázquez-Vílchez, M., Martínez-Martínez, J. M., & Gabites, J. (2015). The structure of the Temsamane fold-and-thrust stack (eastern Rif, Morocco): Evolution of a transpressional orogenic wedge. *Tectonophysics*, *663*, 150–176. https://doi.org/10.1016/j.tecto.2015.02.003

Jones, T., & Nur, A. (1984). Seismic velocity and anisotropy in mylonites and the reflectivity of deep crustal fault zones. *Geology*, *10*(5), 260–263. https://doi.org/10.1130/0091-7613(1982)10<260:SVAAIM>2.0.CO;2

Kelley, S. P., & Platt, J. (1999). Ar-Ar dating of biotite and muscovite from Alboran basement samples, site 976. *Proceeding of the Ocean Drilling Program, Scientific Results*, *161*, 301–305. https://doi.org/10.2973/odp.proc.sr.161.215.1999

Klemperer, S. L., & Matthews, D. H. (1987). Lapetus suture located beneath the North Sea by BIRPS deep seismic reflection profiling, (March). *Geology*, *15*, 195–198.

Knapp, J. H., Steer, D. N., Brown, L. D., Berzin, R., Suleimanov, A., Stiller, M., et al. (1996). Lithosphere-scale seismic image of the southern Urals from explosion-source reflection profiling. *Science*, *274*(5285), 226–228. https://doi.org/10.1126/science.274.5285.226

Lonergan, L., & White, N. (1997). Origin of the Betic-Rif mountain belt. *Tectonics*, *16*, 504–522. https://doi.org/10.1029/96TC03937

Luján, M., Crespo-Blanc, A., & Balanyá, J. (2006). The Flysch Trough thrust imbricate (Betic Cordillera): A key element of the Gibraltar Arc orogenic wedge. *Tectonics*, *25*, TC6001. https://doi.org/10.1029/2005TC001910

Mancilla, F. d. L., Booth-Rea, G., Stich, D., Pérez-Peña, J. V., Morales, J., Azañón, J. M., et al. (2015). Slab rupture and delamination under the Betics and Rif constrained from receiver functions. *Tectonophysics*, *663*, 225–237. https://doi.org/10.1016/j.tecto.2015.06.028

Mancilla, F. d. L., & Diaz, J. (2015). High resolution Moho topography map beneath Iberia and northern Morocco from receiver function analysis. *Tectonophysics*, *663*, 203–211. https://doi.org/10.1016/j.tecto.2015.06.017

Marchesi, C., Garrido, C. J., Bosch, D., Bodinier, J. L., Hidas, K., Padrón-Navarta, J. A., & Gervilla, F. (2012). A Late Oligocene Suprasubduction setting in the westernmost Mediterranean revealed by intrusive pyroxenite dikes in the Ronda Peridotite (southern Spain). *The Journal of Geology*, *120*(2), 237–247. https://doi.org/10.1086/663875

Martínez-García, P., Comas, M., Lonergan, L., & Watts, A. B. (2017). From extension to shortening: Tectonic inversion distributed in time and space in the Alboran Sea, Western Mediterranean. *Tectonics*, *36*, 2777–2805. https://doi.org/10.1002/2017TC004489

Martínez-García, P., Comas, M., Soto, J. I., Lonergan, L., & Watts, A. B. (2013). Strike-slip tectonics and basin inversion in the western Mediterranean: The post-Messinian evolution of the Alboran Sea. *Basin Research*, *25*(4), 361–387. https://doi.org/10.1111/bre.12005

Martínez-Loriente, S., Bartolome, R., Perea, H., Klaeschen, D., Zitellini, N., Wynn, R. B., & Masson, D. G. (2016). Morphostructure, tectono-sedimentary evolution and seismic potential of the Horseshoe Fault, SW Iberian margin, (5). *Basin Research*, *30*, 382–400. https://doi.org/10.1111/bre.12225

Martínez-Loriente, S., Gràcia, E., Bartolome, R., Sallarès, V., Connors, C., Perea, H., et al. (2013). Active deformation in old oceanic lithosphere and significance for earthquake hazard: Seismic imaging of the Coral Patch Ridge area and neighboring abyssal plains (SW Iberian margin). *Geochemistry, Geophysics, Geosystems*, *14*, 2206–2231. https://doi.org/10.1002/ggge.20173

Martínez-Loriente, S., Sallarès, V., Gràcia, E., Bartolome, R., Dañobeitia, J. J., & Zitellini, N. (2014). Seismic and gravity constraints on the nature of the basement in the Africa-Eurasia plate boundary: New insights for the geodynamic evolution of the SW Iberian margin. *Journal of Geophysical Research: Solid Earth*, *119*, 567–580. https://doi.org/10.1002/2013JB010601

Matthews, D. H. (1982). BIRPS: Deep seismic reflection profiling around the British Isles. *Nature*, *298*(5876), 709–710. https://doi.org/10.1038/298709a0

Medaouri, M., Déverchère, J., Graindorge, D., Bracene, R., Badji, R., Ouabadi, A., et al. (2014). The transition from Alboran to Algerian basins (western Mediterranean Sea): Chronostratigraphy, deep crustal structure and tectonic evolution at the rear of a narrow slab rollback system. *Journal of Geodynamics*, *77*, 186–205. https://doi.org/10.1016/j.jog.2014.01.003

Meissner, R., Luschen, E., & Flüh, E. R. (1983). Studies of the continental crust by near-vertical reflection methods: A review. *Physics of the Earth and Planetary Interiors*, *31*(4), 363–376. https://doi.org/10.1016/0031-9201(83)90095-X

Monk, D. J. (1993). Wave-equation multiple suppression using constrained gross equalization. *Geophysical Prospecting*, *41*(6), 725–736. https://doi.org/10.1111/j.1365-2478.1993.tb00880.x

Moreno, X., Gràcia, E., Bartolome, R., Martínez-Loriente, S., Perea, H., Gómez de la Peña, L., et al. (2016). Seismostratigraphy and tectonic architecture of the Carboneras Fault offshore based on multiscale seismic imaging: Implications for the Neogene evolution of the NE Alboran Sea. *Tectonophysics*, *689*, 115–132. https://doi.org/10.1016/j.tecto.2016.02.018

Negro, F., Agard, P., Goffe, B., & Saddiqi, O. (2007). Tectonic and metamorphic evolution of the Temsamane units, External Rif (northern Morocco): Implications for the evolution of the Rif and the Betic-Rif arc. *Journal of the Geological Society*, *164*, 829–842.

Negro, F., de Sigoyer, J., Goffé, B., Saddiqi, O., & Villa, I. M. (2008). Tectonic evolution of the Betic—Rif arc: New constraints from 40 Ar/39 Ar dating on white micas in the Temsamane units (External Rif, northern Morocco). *Lithos*, *106*(1–2), 93–109. https://doi.org/10.1016/j.lithos.2008.06.011

Palomeras, I., Thurner, S., Levander, A., Liu, K., Villaseñor, A., Carbonell, R., & Harnafi, M. (2014). Finite-frequency Rayleigh wave tomography of the western Mediterranean: Mapping its lithospheric structure. *Geochemistry, Geophysics, Geosystems*, *15*, 140–160. https://doi.org/10.1002/2013GC004861

Palomeras, I. V., Thurner, S., Levander, A., Gallart, J., & Harnafi, M. (2017). Lithospheric structure of Iberia and Morocco using finite-frequency Rayleigh wave tomography from earthquakes and seismic ambient noise I. *Geochemistry, Geophysics, Geosystems*, *18*, 1824–1840. https://doi.org/10.1002/2016GC006657

Platt, J. P. (2007). From orogenic hinterlands to Mediterranean-style back-arc basins: A comparative analysis. *Journal of the Geological Society*, *164*(2), 297–311. https://doi.org/10.1144/0016-76492006-093

Platt, J. P., Behr, W. M., Johanesen, K., & Williams, J. R. (2013). The Betic-Rif Arc and its orogenic hinterland: A review. *Annual Review of Earth and Planetary Sciences*, *41*(1), 313–357. https://doi.org/10.1146/annurev-earth-050212-123951

Ranero, C. R., Banda, E., & Buhl, P. (1997). The crustal structure of the Canary Basin: Accretion processes at slow spreading centers. *Journal of Geophysical Research*, *102*, 10,185–10,201. https://doi.org/10.1029/97JB00101

Ranero, C. R., & Pérez-Gussinyé, M. (2010). Sequential faulting explains the asymmetry and extension discrepancy of conjugate margins. *Nature*, *468*(7321), 294–299. https://doi.org/10.1038/nature09520

Ranero, C. R., Reston, T. J., Belykh, I., & Gnibidenko, H. (1997). Reflective oceanic crust formed at a fast-spreading center in the Pacific. *Geology*, *25*(6), 499–502. https://doi.org/10.1130/0091-7613(1997)025<0499:ROCFAA>2.3.CO;2

Rosenbaum, G., Lister, G. S., & Duboz, C. (2002). Reconstruction of the tectonic evolution of the western Mediterranean since the Oligocene. *Journal of the Virtual Explorer*, *8*, 107–126.

Rutter, E. H., Faulkner, D. R., & Burgess, R. (2012). Structure and history Carboneras Fault Zone: Part of a stretching transform system. *Journal of Structural Geology*, *42*, 227. https://doi.org/10.1016/j.jsg.2012.05.001

Sallarès, V., Gailler, A., Gustscher, M. A., Graindorge, D., Bartolome, R., Gràcia, E., et al. (2011). Seismic evidence for the presence of Jurassic oceanic crust in the central Gulf of Cadiz (SW Iberian margin). *Earth and Planetary Science Letters*, *311*, 112–123.

Sallarès, V., Martínez-Loriente, S., Prada, M., Gràcia, E., Ranero, C., Gutscher, M. A., et al. (2013). Seismic evidence of exhumed mantle rock basement at the Gorringe Bank and the adjacent Horseshoe and Tagus abyssal plains (SW Iberia). *Earth and Planetary Science Letters*, *365*, 120–131. https://doi.org/10.1016/j.epsl.2013.01.021

Sanz De Galdeano, C. (1990). Geologic evolution of the Betic Cordilleras in the western Mediterranean, Miocene to the present. *Tectonophysics*, *172*(1–2), 107–119. https://doi.org/10.1016/0040-1951(90)90062-D

Scotney, P., Burgess, R., & Rutter, E. (2000). 40Ar/39Ar age of the Cabo de Gata volcanic series and displacements on the Carboneras fault zone, SE Spain. *Journal of The Geological Society - J Geol Soc*, *157*(5), 1003–1008. https://doi.org/10.1144/jgs.157.5.1003

Seber, D., Barazangi, M., Ibenbrahim, A., & Demnati, A. (1996). Geophysical evidence for lithospheric delamination beneath the Alboran Sea and Rif-Betic mountains. *Nature*, *379*(6568), 785–790. https://doi.org/10.1038/379785a0

Sosson, M., Morillon, A., Bourgois, J., Frraud, G., Poupeau, G., & Saint-marc, P. (1998). Late exhumation stages of the Alpujarride Complex (western Betic Cordilleras, Spain): New thermochronological and structural data on Los Reales and Ojen nappes. *Tectonophysics*, *285*(3-4), 253–273. https://doi.org/10.1016/S0040-1951(97)00274-6

Spakman, W., & Wortel, R. (2004). A tomographic view on western Mediterranean Geodynamics. *The TRANSMED Atlas, The Mediterranean Region from Crust to Mantle*, 31–52. https://doi.org/10.1007/978-3-642-18919-7_2

Torelli, L., Sartori, R., & Zitellini, N. (1997). The giant chaotic body in the Atlantic Ocean off Gibraltar: New results from a deep seismic reflection survey. *Marine and Petroleum Geology*, *14*, 125–134. https://doi.org/10.1016/S0264-8172(96)00060-8

Torres-Roldan, R. L., Poli, G., & Peccerillo, A. (1986). An early Miocene arc-tholeitic magmatic dyke event from the Alboran Sea: Evidence for precollision subduction and back-arc crustal extension in the westernmost Mediterranean. *Geologische Rundschau*, *75*(1), 219–234. https://doi.org/10.1007/BF01770190

Van Hinsbergen, D. J. J., Vissers, R. L. M., & Spakman, W. (2014). Origin and consequences of western Mediterranean subduction, rollback, and slab segmentation. *Tectonics*, *33*, 393–419. https://doi.org/10.1002/2013TC003349

Wang, Y. (2003). Multiple subtraction using an expanded multichannel matching filter. *Geophysics*, *68*(1), 346–354. https://doi.org/10.1190/1.1543220

Watts, A. B., Platt, J. P., & Buhl, P. (1993). Tectonic evolution of the Alboran Sea basin. *Basin Research*, *5*(3), 153–177. https://doi.org/10.1111/j.1365-2117.1993.tb00063.x

Wessel, P., & Smith, W. H. F. (1991). Free software helps map and display data. *Eos, Transactions American Geophysical Union*, *72*(41), 441–446. https://doi.org/10.1029/90EO00319

Wortel, M. J., & Spakman, W. (2000). Subduction and slab detachment in the Mediterranean-Carpathian region. *Science*, *290*(5498), 1910–1917. https://doi.org/10.1126/science.290.5498.1910

Yilmaz, O. (1987). Seismic data analysis: Processing, Inversion and Interpretation of seismic data. Society of Exploration Geophysicists, 2027 p.

Zitellini, N., Gràcia, E., Matias, L., Terrinha, P., Abreu, M. A., De Alteriis, G., et al. (2009). The quest for the Africa-Eurasia plate boundary west of the Strait of Gibraltar. *Earth and Planetary Science Letters*, *280*(1–4), 13–50. https://doi.org/10.1016/j.epsl.2008.12.005